

1 **MRGPRX4 is a novel bile acid receptor in cholestatic itch**

2 Huasheng Yu<sup>1,2,3</sup>, Tianjun Zhao<sup>1,2,3</sup>, Simin Liu<sup>1</sup>, Qinxue Wu<sup>4</sup>, Omar Johnson<sup>4</sup>, Zhaofa  
3 Wu<sup>1,2</sup>, Zihao Zhuang<sup>1</sup>, Yaocheng Shi<sup>5</sup>, Renxi He<sup>1,2</sup>, Yong Yang<sup>6</sup>, Jianjun Sun<sup>7</sup>,  
4 Xiaoqun Wang<sup>8</sup>, Haifeng Xu<sup>9</sup>, Zheng Zeng<sup>10</sup>, Xiaoguang Lei<sup>3,5</sup>, Wenqin Luo<sup>4\*</sup>, Yulong  
5 Li<sup>1,2,3\*</sup>

6

7 <sup>1</sup>State Key Laboratory of Membrane Biology, Peking University School of Life  
8 Sciences, Beijing 100871, China

9 <sup>2</sup>PKU-IDG/McGovern Institute for Brain Research, Beijing 100871, China

10 <sup>3</sup>Peking-Tsinghua Center for Life Sciences, Beijing 100871, China

11 <sup>4</sup>Department of Neuroscience, Perelman School of Medicine, University of  
12 Pennsylvania, Philadelphia, PA 19104, USA

13 <sup>5</sup>Department of Chemical Biology, College of Chemistry and Molecular Engineering,  
14 Peking University, Beijing 100871, China

15 <sup>6</sup>Department of Dermatology, Peking University First Hospital, Beijing Key Laboratory  
16 of Molecular Diagnosis on Dermatoses, Beijing 100034, China

17 <sup>7</sup>Department of Neurosurgery, Peking University Third Hospital, Peking University,  
18 Beijing, 100191, China

19 <sup>8</sup>State Key Laboratory of Brain and Cognitive Science, CAS Center for Excellence in  
20 Brain Science and Intelligence Technology (Shanghai), Institute of Biophysics,  
21 Chinese Academy of Sciences, Beijing, 100101, China

22 <sup>9</sup>Department of Liver Surgery, Peking Union Medical College Hospital, Chinese

23 Academy of Medical Sciences and Peking Union Medical College, Beijing 100730,

24 China

25 <sup>10</sup>Department of Infectious Diseases, Peking University First Hospital, Beijing 100034,

26 China

27 \*Manuscript correspondence:

28 Yulong Li ([yulongli@pku.edu.cn](mailto:yulongli@pku.edu.cn)) & Wenqin Luo ([luow@penmedicine.upenn.edu](mailto:luow@penmedicine.upenn.edu))

29

30 **Acknowledgments:** We thank Dr. Y. Rao for sharing the tissue culture room, Dr. J.H.

31 Zhao for collecting clinical blood samples. We are grateful to Dr. L.Q. Luo and Dr. Y.

32 Song for critical reading of the manuscript. We also thank Dr. X.Z. Dong for sharing

33 unpublished data. This work was supported by the Junior Thousand Talents Program

34 of China to Y.L.

35

36

37

38

39

40

41

42

43 **Abstract:**

44 Patients with liver diseases often suffer from chronic itch or pruritus, yet the  
45 itch-causing pruritogen(s) and their cognate receptor(s) remain largely elusive. Using  
46 transcriptomics and GPCR activation assays, we found that an orphan, primate  
47 specific MRGPRX4 is expressed in human dorsal root ganglia (hDRG) and selectively  
48 activated by bile acids. *In situ* hybridization and immunohistochemistry revealed that  
49 MRGPRX4 is expressed in ~7% of hDRG neurons and co-localizes with HRH1, a  
50 known itch-inducing GPCR. Bile acids elicited a robust Ca<sup>2+</sup> response in a subset of  
51 cultured hDRG neurons, and intradermal injection of bile acids and an MRGPRX4  
52 specific agonist induced significant itch in healthy human subjects. Surprisingly,  
53 application of agonist for TGR5, a known sequence conserved bile acid receptor  
54 previously implicated in cholestatic itch, failed to elicit Ca<sup>2+</sup> response in cultured  
55 hDRG neurons, nor did it induce pruritus in human subjects. *In situ* hybridization and  
56 immunostaining results revealed that hTGR5 is selectively expressed in satellite glial  
57 cells, unlike mTGR5 (in mouse DRG neurons), likely accounting for the inter-species  
58 difference functionally. Finally, we found that patients with cholestatic itch have  
59 significantly higher plasma bile acid levels compared to non-itchy patients and the bile  
60 acid levels significantly decreased after itch relief. This elevated bile acid level in itchy  
61 patients is sufficient to activate MRGPRX4. Taken together, our data strongly suggest  
62 that MRGPRX4 is a novel bile acid receptor that likely underlies cholestatic itch,  
63 providing a promising new drug target for anti-itch therapies.

64

## 65 INTRODUCTION

66 Chronic itch, or pruritus, is a severe and potentially debilitating clinical feature  
67 associated with many dermatological and systemic conditions<sup>1</sup>, severely affecting  
68 quality of life and potentially leading to lassitude, fatigue, and even depression and  
69 suicidal tendencies<sup>2</sup>. The most well-characterized itch receptors are the H1 and H4  
70 histamine receptors (HRH1 and HRH4)<sup>3</sup>. Although antihistamines, which act by  
71 inhibiting histamine receptors, are generally effective at relieving itch symptoms  
72 induced by inflammation and allergens, these compounds are usually ineffective at  
73 treating chronic itch caused by systemic diseases and most skin disorders. To date,  
74 no effective treatment is available for treating histamine-resistant itch<sup>2</sup>.

75 A high percentage of patients with systemic liver failure develop itch with  
76 cholestatic symptoms<sup>4</sup>. For example, the prevalence of itch is as high as 69% among  
77 patients with primary biliary cirrhosis, and severe itch is an indication for liver  
78 transplantation<sup>5</sup>. Moreover, itch occurs in more than half of pregnant woman with  
79 intrahepatic cholestasis of pregnancy, a condition that has been associated with an  
80 increased risk of preterm delivery, perinatal mortality, and fetal distress<sup>6</sup>.

81 Several medications have been tested for treating cholestatic itch, including  
82 ursodeoxycholic acid (UDCA), cholestyramine, and rifampicin; however, these  
83 compounds either are ineffective or induce severe side effects<sup>5</sup>. Therefore, safe and  
84 effective treatments for cholestatic itch are urgently needed, and identifying the  
85 underlying molecular mechanisms—particularly the receptor and ligand—is the  
86 essential first step.

87 Although the link between cholestasis and itch was first described more than

88 2000 years ago<sup>7</sup>, the detailed mechanisms underlying cholestatic itch remain  
89 unidentified. To date, a handful of molecules have been proposed as the pruritogens  
90 that mediate cholestatic itch, including bile acids, bilirubin, lysophosphatidic acid,  
91 autotaxin, and endogenous opioids<sup>4</sup>. With respect to the cognate receptor for the  
92 pruritogen, a few receptors have been proposed, albeit based primarily on rodent  
93 models. For example, the membrane-bound bile acid receptor TGR5 has been  
94 reported to mediate bile acid-induced itch in mice<sup>8,9</sup>. However, a recent study found  
95 that administering TGR5-selective agonists failed to elicit an itch response in mouse  
96 models of cholestasis<sup>10</sup>, raising doubts regarding whether TGR5 is indeed the  
97 principal mediator for cholestatic itch. Recently, Meixiong et al. reported that Mrgpra1  
98 and MRGPRX4 (in mice and humans, respectively) can be activated by bilirubin, a  
99 compound that serves as one of the pruritogens in cholestatic itch in mice<sup>11</sup>.  
100 Nevertheless, the precise molecular mechanism that underlie cholestatic itch in  
101 humans remains to be determined.

102 We specifically focused our search on genes that are selectively expressed in the  
103 human dorsal root ganglia (DRG), where the cell bodies of primary itch-sensing  
104 neurons are located. Our search revealed a novel ligand-receptor pair comprised of  
105 bile acids (the ligand) and the receptor MRGPRX4. Moreover, we found that  
106 MRGPRX4 is expressed selectively in a small subset of neurons in the human DRG,  
107 and bile acids directly trigger intracellular Ca<sup>2+</sup> increase in these neurons. In addition,  
108 intradermal injection of both bile acids and the MRGPRX4-specific agonist nateglinide  
109 induce detectable itch in human subjects, and this bile acid-induced itch is

110 histamine-independent. Surprisingly, application of agonist for TGR5, a known  
111 sequence conserved bile acid receptor previously implicated in cholestatic itch, failed  
112 to elicit  $\text{Ca}^{2+}$  response in cultured hDRG neurons, nor did it induce pruritus in human  
113 subjects. In situ hybridization and immunostaining results revealed that unlike  
114 mTGR5 expressing in mouse DRG neurons, hTGR5 is selectively expressed in  
115 satellite glial cells, likely accounting for the inter-species difference functionally.  
116 Finally, we found that plasma bile acid levels are well correlated with itch sensation in  
117 cholestatic patients and that this elevated bile acid level is sufficient to activate  
118 MRGPRX4. Taken together, our results provide compelling evidence that the  
119 ligand-receptor pair of bile acids and MRGPRX4 is likely to be one of the critical  
120 mediators for human cholestatic itch.

121

## 122 **RESULTS**

### 123 ***MRGPRX4 is activated by bile extract***

124 DRG neurons are primary somatosensory neurons that express a variety of receptors  
125 and ion channels for detecting both extrinsic and intrinsic stimuli<sup>12</sup>. To identify a  
126 receptor in mediating cholestatic itch in human, we reason that this candidate  
127 receptor could be expressed in human DRG neurons and activated by bile extracts.  
128 Since the majority of itch receptors identified to date belong to the G protein-coupled  
129 receptor (GPCR) superfamily<sup>13</sup>, we analyzed two published transcriptomics datasets  
130 compiled from a variety of human tissues<sup>14,15</sup>, specifically focusing on GPCRs.  
131 Among the 332 transcripts that are enriched in the human DRG (Table S1), we

132 identified the following seven highest-enriched orphan GPCRs: GPR149, MRGPRX4,  
133 GPR139, GPR83, MRGPRES, MRGPRX1, and MRGPRD<sup>16,17</sup> (**Fig. 1a and Table S2**).  
134 Next, we cloned and expressed these candidate receptors in HEK293T cells  
135 (**Supplementary Fig. 1a, b**), finding that all seven receptors were expressed at the  
136 plasma membrane (**Supplementary Fig. 1b**). We measured the activation of each  
137 receptor by bovine bile extract using two reporter assays, the Gs-dependent  
138 luciferase assay<sup>18</sup> and the Gq-dependent TGF $\alpha$  shedding assay<sup>19</sup> (**Fig. 1b,c**). No  
139 signal was detected with the Gs-dependent luciferase assay (**Fig. 1b**). Interestingly,  
140 bile extract elicited a significant increase in reporter activity in cells expressing  
141 MRGPRX4 measured using the TGF $\alpha$  shedding assay, but had no effect on cells  
142 expressing the other six GPCRs (**Fig. 1c**). These results suggest that MRGPRX4 is  
143 activated by one or more compounds present in bile extract, and that MRGPRX4  
144 likely signals through the Gq but not the Gs pathway. Further experiments revealed  
145 that bovine, porcine, and human bile extract activate MRGPRX4 to a similar extent in  
146 a dose-dependent manner (**Fig. 1d**); in contrast, extracts obtained from bovine brain,  
147 spleen, heart, kidney, and liver tissues induced no detectable signal on  
148 MRGPRX4-expressing cells (**Fig. 1e**). Taken together, these results suggest that  
149 MRGPRX4 is potently activated by bile extract and active compound(s) is/are highly  
150 enriched in bile extract.

151

### 152 ***Identifying which in bile extract activate MRGPRX4***

153 Next, to identify the component(s) in bovine bile extract that activate(s) MRGPRX4,

154 we separated the extract into six fractions using silica gel column chromatography  
155 (**Fig. 2a**). Each fraction was then applied to MRGPRX4-expressing HEK293T cells,  
156 and MRGPRX4 activation was measured using the TGF $\alpha$  shedding assay. Among the  
157 six fractions tested, fraction 4 caused the strongest activation of MRGPRX4, whereas  
158 fractions 1 and 6 caused the weakest activity (**Fig. 2b**), indicating that the active  
159 component(s) are mainly present in fraction 4. Mass spectrometry of fractions 4 and 6  
160 revealed a peak enriched specifically in fraction 4 (**Fig. 2c**); this peak corresponded to  
161 ions with an m/z value of 410.3265 in the positive ion mode and was annotated to  
162 prostaglandin F $2\alpha$  diethyl amide and/or dihydroxy bile acids. Further experiments  
163 using  $^1\text{H-NMR}$  revealed that two pure dihydroxy bile acids—deoxycholic acid (DCA)  
164 and chenodeoxycholic acid (CDCA)—produced peaks that were identical to the  
165 peaks in fraction 4 (**Fig. 2d**); other fractions that only weakly activated MRGPRX4  
166 also contained characteristic peaks of bile acids as shown by  $^1\text{H-NMR}$   
167 (**Supplementary Fig. 2**). These results suggest that DCA and/or CDCA are enriched  
168 in the active fraction of bile extract and may be the key compounds that activate  
169 MRGPRX4.

170

### 171 ***Characterization of bile acids: MRGPRX4 activation and the downstream*** 172 ***signaling***

173 To further characterize the efficacy and potency of DCA, CDCA, other bile acids, and  
174 their derivatives in activating MRGPRX4, we systematically measured their ability to  
175 activate MRGPRX4 in HEK293T cells, using TGF $\alpha$  shedding assay and FLIPR



176 (fluorescent imaging plate reader)  $\text{Ca}^{2+}$  assay. All of the bile acids tested activated  
177 MRGPRX4 to some extent; DCA had the highest potency measured with both assays,  
178 with an  $\text{EC}_{50}$  value of 2.7  $\mu\text{M}$  and 2.6  $\mu\text{M}$  in the TGF $\alpha$  shedding and FLIPR assays,  
179 respectively; cholic acid (CA), CDCA, and lithocholic acid (LCA)—three close analogs  
180 of DCA—were less potent (**Fig. 3a-c**). Based on the structural differences between  
181 DCA and the less potent bile acids, we reasoned that hydroxylation at position of R1  
182 and/or R2, as well as taurine/glycine conjugation at position R3, is important for  
183 specific bile acids to activate MRGPRX4 (**Fig. 3c**).

184 Next, we examined the potential signaling events downstream of bile  
185 acid-induced MRGPRX4 activation by measuring intracellular  $\text{Ca}^{2+}$  concentration  
186 ( $[\text{Ca}^{2+}]_i$ ) in MRGPRX4-expressing HEK293T cells loaded with Fluo-8 AM, a  
187 fluorescent  $\text{Ca}^{2+}$  indicator. We found that DCA, CA, CDCA, and LCA induced a robust  
188 fluorescence response in these cells (**Fig. 3d-f**), and pretreating the cells with the  
189 phospholipase C inhibitor U73122 significantly reduced the DCA-evoked  $\text{Ca}^{2+}$  signals;  
190 in contrast, the G $\beta\gamma$  inhibitor gallein had no effect on DCA-evoked signaling (**Fig.**  
191 **3g-h**). Taken together, these results indicate that a Gq-dependent signaling pathway  
192 involving phospholipase C is downstream to MRGPRX4 activation by bile acids.

193 Interestingly, even though MRGPRX1, MRGPRX2, and MRGPRX3 are close  
194 analogs of MRGPRX4, none of these receptors was activated by bile acids, even at  
195 100  $\mu\text{M}$  concentration (**Supplementary Fig. 3a-e**). We therefore investigated the  
196 putative ligand-binding sites in MRGPRX4 by comparing the primary amino acid  
197 sequence of MRGPRX4 with these three analogs (**Fig. 3i**). We identified amino acid

198 residues that are conserved in MRGPRX1, MRGPRX2, and MRGPRX3 but not in  
199 MRGPRX4 and mutated these residues, once per time, to an alanine residue in  
200 MRGPRX4. We found that mutating amino acids 159, 180, and 235 reduced the  
201 receptor's affinity for DCA (**Fig. 3j**), without affecting trafficking to the cell membrane  
202 (**Fig. 3k**); thus, these three sites may play a critical role in the binding of bile acids to  
203 MRGPRX4. In addition, we examined whether mouse and/or rat Mrgpr family  
204 members also respond to bile acids. Intriguingly, bile acids failed to activate any  
205 mouse or rat Mrgpr members tested (**Supplementary Fig. 3g-h**), suggesting that the  
206 ability of MRGPRX4 to sense bile acids may be a new functional addition during  
207 evolution.

208

209 ***A subset of human itch-related DRG neurons express MRGPRX4 and respond***  
210 ***to bile acids***

211 Next, we examined endogenous expression pattern of MRGPRX4 in hDRGs. We  
212 performed *in situ* hybridization using a digoxigenin-labeled riboprobe against  
213 *MRGPRX4* mRNA, and found that *MRGPRX4* mRNA is expressed in only ~6-8% of  
214 hDRG neurons (**Fig. 4a, c**); similar results were obtained with immunofluorescence  
215 using an MRGPRX4-specific antibody (**Fig. 4b, c** and **Supplementary Fig. 4**).  
216 Morphologically, these MRGPRX4-expressing neurons are small-diameter neurons,  
217 with a diameter of approximately 50  $\mu\text{m}$ , which is similar to small-diameter neurons  
218 that express the neurotrophic tyrosine kinase receptor type 1 (TrkA) (**Fig. 4d**),  
219 suggesting a function in nociception and/or pruriception<sup>20</sup>.

220 To further characterize the molecular profile of these MRGPRX4-positive hDRG  
221 neurons, we performed triple-labeling of MRGPRX4 and two additional molecular  
222 markers using RNAscope *in situ* hybridization (**Fig. 4e**). Our analysis revealed  
223 that >90% of MRGPRX4-positive neurons also express the histamine receptor HRH1,  
224 a well-characterized itch receptor in humans<sup>21</sup>, and TRPV1 (transient receptor  
225 potential cation channel subfamily V member 1) (**Fig. 4f-g**), which functions  
226 downstream of Mrgprs and histamine receptors<sup>22,23</sup>. Interestingly, the majority of  
227 MRGPRX4-expressing neurons also co-express Nav1.7 voltage-gated sodium  
228 channel, the peptidergic marker CGRP (calcitonin gene-related peptide), and  
229 TrkA<sup>24,25</sup> (**Fig. 4f-g**). These results suggest that MRGPRX4 is specifically expressed  
230 in a subset of small diameter peptidergic hDRG neurons.

231 Next, we tested whether MRGPRX4 in DRG neurons can be activated by bile  
232 acids. Because bile acids failed to induce a detectable Ca<sup>2+</sup> signal in cultured rat  
233 DRG neurons (**Supplementary Fig. 5**), we expressed the human MRGPRX4 in  
234 cultured rat DRG neurons. Bile acids triggered a robust Ca<sup>2+</sup> response in  
235 MRGPRX4-expressing rat DRG neurons (**Supplementary Fig. 5**), indicating that  
236 MRGPRX4 expressed in rat DRG neurons mediates the bile acid-induced activation.  
237 Consistent with our finding that DCA is a more potent agonist of MRGPRX4 than CA,  
238 DCA induced a significantly larger Ca<sup>2+</sup> response and activated a larger number of  
239 MRGPRX4-expressing rat DRG neurons than CA (**Supplementary Fig. 5**).

240 Next, we asked whether hDRG neurons can also be activated by bile acids.  
241 Application of DCA induced a robust fluorescence increase in a subset (~6%) of these

242 hDRG neurons loaded with Fluo-8 AM; this percentage of DCA-responsive cells is  
243 similar to the percentage of MRGPRX4-expressing cells measured with *in situ*  
244 hybridization (**Fig. 4a, c**). Moreover, the less potent MRGPRX4 agonist CA also  
245 induced a response, albeit much weaker than DCA (**Fig. 4h** and **Supplementary Fig.**  
246 **6**). In addition, nearly all (~90%) of DCA-responsive hDRG neurons were  
247 capsaicin-sensitive, and approximately one-third of DCA-responsive neurons also  
248 responded to histamine (**Fig. 4j**). Together, our results indicate that expression of  
249 MRGPRX4 is sufficient to render bile acid sensitivity of primary somatosensory  
250 neurons.

251

### 252 ***Pharmacological activation of MRGPRX4 triggers itch sensation in human*** 253 ***subjects***

254 Given the specific expression pattern of MRGPRX4 in a subset of hDRG neurons,  
255 and the known role of Mrgpr family members in mediating itch sensation, we next  
256 asked whether pharmacologically activating MRGPRX4 could trigger itch sensation in  
257 human subjects. We recruited healthy volunteers and performed a double-blind skin  
258 itch test, in which each subject received a 25- $\mu$ l intradermal injection of the test  
259 compounds or vehicle in four separate sites on both forearms (**Fig. 5a1, inset**), after  
260 which the subject was asked to rank the itch sensation at each injection site using a  
261 generalized labeled magnitude scale (LMS)<sup>26</sup>. Interestingly, the pharmacological  
262 MRGPRX4 specific agonist nateglinide, a previously reported MRGPRX4 agonist<sup>27</sup>,  
263 (**Supplementary Fig. 3f**) —but not vehicle—induced a robust itch sensation in

264 healthy subjects (**Fig. 5a1, a2**). These results show that activation of MRGPRX4 is  
265 sufficient to trigger itch sensation in humans, suggesting that MRGPRX4 is a human  
266 itch receptor.

267

### 268 ***Bile acid-induced itch in humans is both histamine- and TGR5-independent***

269 Previous studies have implicated that bile acids could induce itch in human<sup>28,29</sup>. Here,  
270 we systematically test pruritic effect of bile acids on human and whether bile acid-  
271 induced itch shows some features similar to that of cholestatic itch<sup>17</sup>. We found that  
272 500 µg (25 µl) of DCA induced a significant itch sensation that peaked within 5 min  
273 and declined slowly over time; in contrast, control injections with vehicle did not  
274 induce an itch response (**Fig. 5a1, a2**). Moreover, itch intensity induced by DCA was  
275 in a dose-dependent manner (**Fig. 5b1, b2**). We also found that less potent  
276 MRGPRX4 agonists, including CA, CDCA, taurochenodeoxycholic acid (TCDCA),  
277 and LCA, also induced a weaker—albeit still significant—itch sensation (**Fig. 5c1, c2**).  
278 Given that antihistamines are largely ineffective for treating cholestatic itch<sup>4</sup>, we  
279 tested whether itch induced by bile acids can be blocked by antihistamines. We found  
280 that pretreating subjects with an antihistamine prevented histamine-induced itch but  
281 had no effect on DCA-induced itch (**Fig. 5d1, d2**), suggesting that itch induced by bile  
282 acids does not involve histamine signaling. Taken together, these results indicate that  
283 bile acids trigger an itch sensation with features similar to cholestatic itch.

284 In mice, the membrane bile acid receptor TGR5 has been reported to mediate  
285 bile acid-induced itch<sup>8,9</sup>. To test whether bile acid-induced itch in human is also

286 mediated by TGR5, we chose a non-bile acid TGR5 agonist compound 15<sup>30</sup>, which is  
287 nearly 70-fold more potent than DCA in activating human TGR5 and does not activate  
288 human MRGPRX4 (**Fig. 6b, c**). Intradermal injections of 10 µg (25µl) of compound 15  
289 did not induce detectable itch in humans, whereas DCA, as the positive control,  
290 induced significant itch (**Fig. 6a1, a2, d**). These results suggest that TRG5 is not the  
291 receptor mediating bile acid-induced itch. Furthermore, we examined the expression  
292 of TGR5 in the human, monkey, and mouse DRG tissues. Very surprisingly, although  
293 the amino acid sequence of TGR5 is relatively conserved between rodents and  
294 primates (**Supplementary Fig. 7a**), we found the different expression pattern of  
295 TGR5 in DRG tissues. In human and monkey, both *in situ* hybridization and  
296 immunostaining revealed that TGR5 is highly expressed in satellite glial cells  
297 surrounding DRG neurons but not the primary sensory neurons (**Fig. 6e-i and**  
298 **Supplementary Fig. 7**), while in mouse, the same *in situ* probe and antibody  
299 detected the expression of TGR5 in mouse DRG neurons (**Fig. 6f, h and**  
300 **Supplementary Fig. 7c**), similar to the previous publication<sup>8,9</sup>. These results  
301 revealed an interesting species difference in TGR5 expression and function between  
302 mouse and primate. Taken together, our results demonstrate that the function of  
303 TGR5 in human somatosensory system is different from that in mouse, and TGR5 is  
304 not the receptor for mediating bile acid-induced itch in human.

305

306 ***The elevated levels of bile acids in cholestatic itchy patients are sufficient to***  
307 ***activate MRGPRX4***

308 Lastly, to investigate whether bile acids are the pruritogens under pathological  
309 conditions, we collected plasma samples from patients with liver or skin diseases and  
310 measured the concentration of 12 major bile acids using HPLC-MS/MS (**Fig. 7a and**  
311 **Supplementary Fig. 8a**). We found that glycine- and taurine-conjugated primary bile  
312 acids, including glycocholic acid (GCA), taurocholic acid (TCA),  
313 glycochenodeoxycholic acid (GCDCA), and TCDCA are the major bile acids present  
314 in cholestatic patients (**Fig. 7a**), consistent with previously published results<sup>31-33</sup>.  
315 Compared to itchy patients with liver diseases, non-itchy patients had significantly  
316 higher levels of total bile acids (defined here as the sum of the 12 bile acids shown in  
317 **Fig. 7a**) (**Fig. 7a, b**). The level of total plasma bile acids in the itchy patients with skin  
318 diseases was barely detectable and significantly lower than the itchy patients with  
319 liver diseases. Among the 12 bile acids measured, the ones with the largest  
320 differences between the patients with itch and those without itch were for GCA,  
321 GCDCA, TCA, and TCDCA (**Fig. 7a, b**), suggesting that these four bile acids play key  
322 roles in mediating chronic itch under pathological conditions. Indeed, intradermal  
323 injections of TCDCA caused significant itch in healthy subjects (**Fig. 5c1, c2**). For  
324 DCA, the most potent ligand for MRGPRX4 among all tested bile acids, we did not  
325 see the significant difference between itchy and non-itchy patients with liver diseases  
326 (**Fig. 7a**), suggesting it is not the major contributor for cholestatic itch under  
327 pathological conditions. More importantly, although bile acid levels vary among itchy  
328 patients with liver diseases both from our data (**Fig. 7a, b**) and previously reported  
329 results<sup>32-34</sup>, we found that the total plasma bile acids, as well as the individual levels of

330 GCDCA, TCDCA, TCA, and GCA, significantly decreased in 11 out of 13 patients  
331 following itch relief (**Fig. 7c, d** and **Supplementary Fig. 8c**). Taken together, these  
332 results suggest that high levels of bile acids are well correlated with itchy symptom in  
333 patients with liver diseases and that bile acids—particularly GCDCA, TCDCA, TCA,  
334 and GCA— could be main metabolites triggering cholestatic itch.

335 Next, we examined whether combinations of bile acids at pathologically relevant  
336 levels are sufficient to activate MRGPRX4. We prepared mixtures of bile acids similar  
337 to the plasma/serum levels in healthy subjects (“healthy mix”) or in patients with liver  
338 diseases and itch (“liver itch mix”), which are estimated based on previously  
339 published data<sup>31,35</sup> and our quantification results (**Fig. 7a**). These mixtures were then  
340 applied to MRGPRX4-expressing HEK293T cells while performing Ca<sup>2+</sup> imaging. We  
341 found that the “liver itch mix” but not “healthy mix” induced a significant Ca<sup>2+</sup> signal  
342 (**Fig. 7e, f**), suggesting that pathological relevant level of bile acids is sufficient to  
343 activate MRGPRX4.

344 Recently, Meixiong et al. reported that MRGPRX4 can also be activated by  
345 bilirubin, which is another potential pruritogen for triggering cholestatic itch<sup>11</sup>. We  
346 therefore compared bilirubin and DCA with respect to binding and activating  
347 MRGPRX4. We found that compared to bile acids, bilirubin is a less potent, partial  
348 agonist of MRGPRX4 (**Supplementary Fig. 9a**). Given the structural differences  
349 between bilirubin and DCA, we then tested whether bilirubin is an allosteric modulator  
350 of MRGPRX4. Indeed, we found that bilirubin can potentiate the activation of  
351 MRGPRX4 by DCA (**Supplementary Fig. 9b**), and—conversely—DCA potentiate the



352 activation of MRGPRX4 by bilirubin (**Supplementary Fig. 9c**). Moreover, we found  
353 that both total bilirubin and conjugated bilirubin levels were significantly higher in itchy  
354 patients with liver diseases compared to non-itchy patients (**Supplementary Fig. 9d**)  
355 and plasma bilirubin levels decreased significantly after itch relief (**Supplementary**  
356 **Fig. 9e**). Compare to total bilirubin, total bile acids show better correlation with itch  
357 intensity (measured using a self-report numerical rating scale<sup>36</sup>) (**Supplementary Fig.**  
358 **9f**). Taken together, these results suggest that bile acids are the major pruritogens in  
359 MRGPRX4-mediated cholestatic itch and bilirubin facilitates the activation of  
360 MRGPRX4 by bile acids and may also contribute to cholestatic itch in pathological  
361 conditions.

362

## 363 **DISCUSSION**

364 Here, we report that MRGPRX4 is a novel GPCR that fits with the criteria we set for  
365 identifying putative receptor in mediating cholestatic itch. MRGPRX4 is selectively  
366 expressed in a small subset of human DRG neurons. Bile acids triggered a robust  
367 Ca<sup>2+</sup> response in a subset of hDRG neurons as well as rat DRG neurons expressing  
368 MRGPRX4 exogenously. Both bile acids and an MRGPRX4-specific agonist induce  
369 itch in human. Bile acid-induced itch in human is histamine independent, which is  
370 consistent with antihistamines are largely ineffective for treating cholestatic itch.  
371 Surprisingly, application of agonist for TGR5 failed to elicit Ca<sup>2+</sup> response in cultured  
372 hDRG neurons, nor did it induce pruritus in human subjects. The expression pattern  
373 of TGR5 is different between mouse and human. hTGR5 is selectively expressed in

374 satellite glial cells, while mTGR5 is expressed in DRG neurons, likely accounting for  
375 the inter-species difference functionally. We also found that plasma levels of bile  
376 acids were well correlated with itchy patients with liver diseases. Importantly, a  
377 mixture of bile acids with components and concentrations similar to that of cholestatic  
378 itchy patients—but not healthy volunteers—was sufficient to activate MRGPRX4. Our  
379 data indicate bile acids are the major pruritogens in MRGPRX4-mediated cholestatic  
380 itch and bilirubin facilitates the activation of MRGPRX4 by bile acids and may also  
381 contribute to cholestatic itch in pathological conditions. Based on our results, we  
382 propose a new working model for cholestatic itch (**Fig. 7g**): patients with cholestasis  
383 usually display increased plasma levels of bile acids and bilirubin, which are  
384 precipitated in the skin and activate MRGPRX4 receptors in itch-related primary fibers,  
385 thereby triggering itch in these patients. Our results exclude TGR5 as a primary itch  
386 receptor in human, and the broad expression of TGR5 in satellite glial cells implies a  
387 more general function which remains to be determined in the future.

388 Here, we provide important evidence that MRGPRX4 is sufficient for mediating  
389 bile acid-induced itch, and thus should play an important role in cholestatic itch.  
390 Since specific antagonist for MRGPRX4 is currently unavailable, we could not  
391 determine whether MRGPRX4 is necessary for bile acids induced itch in human.  
392 Future studies will be designed to further examine the role of MRGPRX4 in  
393 cholestatic itch using to-be-developed pharmacological and/or human genetic  
394 approaches. For example, several single-nucleotide polymorphisms (SNPs) have  
395 been identified in the human *MRGPRX4* gene<sup>37</sup>, and it would be interesting to screen

396 for loss-of-function and gain-of-function *MRGPRX4* variants. Characterizing the  
397 relationship between these variants and itch intensity in cholestatic patients and  
398 healthy subjects with bile acid-induced itch could help to further delineate the  
399 relationship between MRGPRX4 activity and cholestatic itch. These experiments will  
400 also help to determine whether MRGPRX4 is the main molecular receptor for  
401 mediating cholestatic itch, or whether other GPCRs<sup>4</sup>, such as lysophosphatidic acid  
402 receptors and serotonin receptors also play roles in cholestatic itch.

403 Our current understandings about mechanisms underlying somatosensation in  
404 the mammalian system are mainly derived from studies of rodents. Despite the great  
405 value and insights we gained using rodent models, notable failures have happened in  
406 translating results obtained in rodents into effective and safe clinical treatments in  
407 human<sup>38-41</sup>. The bile acid receptors we study here is a great example demonstrating  
408 the species differences between rodent and human somatosensory systems.  
409 Although TGR5, a bile acid membrane receptor, was previously reported to be  
410 expressed in mouse DRG neurons and mediate bile acid-induced itch in mice<sup>8,9</sup>, our  
411 expressing characterizations as well as functional assays revealed that TGR5 is not  
412 expressed in human DRG neurons and doesn't directly mediate itch sensation in  
413 human. Instead, primate MRGPRX4 gains the novel function of bile acid sensitivity  
414 during evolution. Therefore, it is crucial to study and validate the mechanism of  
415 cholestatic chronic itch and develop the correspondent treatment within the context of  
416 human physiology.

417 Recently, Meixiong et al. reported that mouse *Mrgpra1* and human MRGPRX4

418 can be activated by bilirubin, suggesting that bilirubin may serve as a pruritogen in  
419 cholestatic itch<sup>11</sup>. Bilirubin, a yellow compound that causes the yellow discoloration in  
420 jaundice, has not been considered a likely candidate pruritogen though, because the  
421 clinical observation that itch often precedes the appearance of jaundice, particularly in  
422 patients with intrahepatic cholestasis of pregnancy (ICP)<sup>42</sup> and patients with primary  
423 biliary cirrhosis<sup>7</sup>. Our results suggest that bilirubin is a partial agonist of MRGPRX4  
424 and may potentiate the activation of MRGPRX4 by bile acids. This notion is  
425 consistent with our finding that the correlation between bile acid levels and itch  
426 intensity is stronger than the correlation between bilirubin levels and itch intensity.  
427 Based on these findings, we propose that bile acid is the major contributor to  
428 cholestatic itch, and bilirubin serves to increase bile acid-induced cholestatic itch  
429 under pathological conditions.

430 In summary, we found that the membrane-bound GPCR MRGPRX4 is a novel bile  
431 acid receptor and may serve as an important molecular mediator of chronic itch in  
432 patients with systemic liver diseases. Our results suggest that MRGPRX4 is a  
433 promising molecular target for developing new treatments to alleviate devastating  
434 chronic itch in these patients.

435

#### 436 **Data availability statement**

437 The data that support the findings of this study are available from the corresponding  
438 author upon request. All figures have associated raw data. There is no restriction  
439 regarding data availability.

440

441 **Conflict of interest**

442 The authors declare no competing interests.

443

444

445

446

447

448 **Figures and legends**

449 **Fig. 1 MRGPRX4 is activated by bile extract.**

450 **(a)** Flow chart for the strategy used to identify orphan GPCRs enriched in human  
451 DRG. Transcriptome analysis of DRG and other tissues (trigeminal ganglia, brain,  
452 colon, liver, lung, skeletal muscle, and testis) revealed 332 transcripts with high  
453 expression in the DRG. The top seven orphan GPCRs are listed. See also  
454 Supplementary Tables S1 and S2. Gene expression data were obtained from Flegel  
455 et al. *PLoS One*, 2013 & 2015.

456 **(b and c)** Activation of MRGPRX4 by bovine bile extract. The diagrams at the top  
457 depict the reporter gene assays used to measure GPCR activation via Gs-dependent  
458 **(b)** and Gq-dependent **(c)** pathways. The seven GPCRs identified in **(a)** were tested,  
459 revealing that MRGPRX4-expressing HEK293T cells are activated by bile extract via  
460 the Gq-dependent pathway. Forskolin and TPA were used as positive controls for  
461 activating Gs- and Gq-dependent signaling, respectively. The responses obtained

462 from the tested GPCRs were normalized to the responses induced by respective  
463 positive controls. As positive controls for detecting GPCR activation, separate cells  
464 were transfected with ADRB1 and stimulated with 10  $\mu$ M norepinephrine (NE) (**b**) or  
465 transfected with HRH1 and stimulated with 10  $\mu$ M histamine (His) (**c**). “HEK (only)”  
466 refers to non-transfected cells. n = 3 experiments performed in triplicate.

467 (**d**) Concentration-response curve for the activation of MRGPRX4 by bovine bile  
468 extract, porcine bile extract, and human bile measured using the TGF $\alpha$  shedding  
469 assay. The bovine and porcine bile extract solutions were diluted 1 :10 from a 100  $\mu$   
470 g/ml stock solution, and the human bile solution was diluted 1:10 from crude human  
471 bile. n = 2 experiments performed in triplicate.

472 (**e**) MRGPRX4 is activated selectively by bovine, porcine, and human bile extracts,  
473 but not by bovine brain, spleen, heart, kidney, or liver tissue extracts. The data for  
474 porcine and human bile are reproduced from (**d**). n = 2 experiments performed in  
475 triplicate. Student's *t*-test, \**p* < 0.05, \*\*\**p* < 0.001, and n.s. not significant (*p* > 0.05).

476

477 **Fig. 2 Identification of the active components in bile extract that activate**  
478 **MRGPRX4.**

479 (**a**) Flow chart depicting the strategy for isolating and identifying candidate MRGPRX4  
480 ligands in bovine bile extract. F1 through F6 indicate the six fractions used in  
481 subsequent experiments.

482 (b) Activation of MRGPRX4 by bile extract fractions F1 through F6; fraction F4 has  
483 the highest activity. The data represent one experiment performed in triplicate.  
484 Student's *t*-test, \*\**p* < 0.01. \*\*\**p* < 0.001 versus fraction F4.

485 (c) MS analysis of fractions F4 and F6 (which showed high and weak activity,  
486 respectively). The selectively enriched peak in fraction F4 at molecular weight  
487 410.3265 corresponds to the bile acids DCA and CDCA.

488 (d) <sup>1</sup>H-NMR analysis of fractions F4 and F6 using purified DCA and CDCA as  
489 controls.

490

491 **Fig. 3 Functional characterization and molecular profiling of bile acids as**  
492 **ligands for MRGPRX4.**

493 (a-c) Dose-dependent activation of MRGPRX4 by various bile acids and their  
494 derivatives. MRGPRX4 activation was measured using the TGF $\alpha$  shedding assay (a)  
495 or the FLIPR assay (b, see methods) in MRGPRX4-expressing HEK293T cells; n = 1  
496 experiment performed in triplicate. The general structure of the bile acids and  
497 derivatives is shown in (a), and the respective potencies of the bile acids/derivatives  
498 are listed in (c).

499 (d-f) Activation of MRGPRX4 by various bile acids in cells loaded with the Ca<sup>2+</sup>  
500 indicator Fluo-8 AM. (d) Representative images of MRGPRX4-expressing HEK293T  
501 cells (shown by mCherry fluorescence) before and after application of 10  $\mu$ M DCA. (e)  
502 Representative traces of Ca<sup>2+</sup> responses induced by application of 10  $\mu$ M DCA, CA,  
503 CDCA, or LCA. n = 50 cells each.

504 **(g-h)** MRGPRX4 is coupled to the Gq-PLC-Ca<sup>2+</sup> signaling pathway. DCA (10 μM)  
505 evoked a robust Ca<sup>2+</sup> signal in MRGPRX4-expressing HEK293T cells **(g, left)**; this  
506 response was blocked by pretreating cells for 30 min with the PLC inhibitor U73122  
507 **(g, middle)**, but not the Gβγ inhibitor gallein **(g, right)**. Triton X-100 was used as a  
508 positive control. The summary data are shown in **(h)**; n = 7-10 cells each. Student's  
509 *t*-test, \*\*\**p* < 0.001, and n.s. = not significant (*p* > 0.05).

510 **(i-k)** Identification of key residues in MRGPRX4 that mediate ligand binding and  
511 receptor activation. **(i)** Primary sequence alignment of the human MRGPRX1,  
512 MRGPRX2, MRGPRX3, and MRGPRX4 proteins. The positions of the three amino  
513 acids in MRGPRX4 that were mutated to alanine are shown at the right. **(j)**  
514 Dose-dependent activation of wild-type (WT) MRGPRX4 and three MRGPRX4  
515 mutants with the indicated point mutations was measured using the TGFα shedding  
516 assay. n = 1 experiment performed in triplicate. **(k)** Plasma membrane expression of  
517 Myc-tagged WT and mutant MRGPRX4 was measured using an anti-Myc antibody  
518 and normalized to WT MRGPRX4 expression.

519

520 **Fig. 4. A subset of human DRG neurons express MRGPRX4 and respond to bile**  
521 **acids.**

522 **(a-d)** Representative DRG sections showing *in situ* hybridization (ISH, **a**) and  
523 immunohistochemistry (IHC, **b**) for MRGPRX4; the summary data are shown in **(c)**; n  
524 = 2234 and 2735 neurons for ISH and IHC, respectively. The scale bars represent  
525 200 μm **(a)** and 100 μm **(b)**. **(d)** Diameter distribution for all 2234 DRG neurons



526 measured using *in situ* hybridization, 124 MRGPRX4-positive neurons, and 788

527 TrkA-positive neurons.

528 **(e)** Flow chart depicting the steps for characterizing the gene expression profiles of

529 human DRG samples using triple-color RNAscope *in situ* hybridization.

530 **(f)** Representative RNAscope images of *MRGPRX4* and other genes in human DRG

531 sections. Each fluorescent dot indicates a single mRNA transcript. Scale bar, 10  $\mu$ m.

532 **(g)** Quantification of the gene expression data shown in **(f)**. A neuron was defined as

533 positive if  $\geq 20$  fluorescent dots in the respective mRNA channel were detected in

534 that neuron.

535 **(h)** Bile acids induced a  $\text{Ca}^{2+}$  response in a subset of cultured human DRG neurons.

536 **(left)** Representative bright-field images and Fluo-8 fluorescence images of two

537 different DRG cultures from one embryo donor one adult donor. **(right)**

538 Representative traces of individual DCA-responsive DRG neurons (circled by the

539 dash line in **(left)**). Pseudo-color images of chemical-induced signals are shown

540 under each trace. C15 (compound 15), CA, DCA, and His (histamine): 100  $\mu$ M each;

541 KCl: 75 mM. Veh, vehicle. Scale bar, 50  $\mu$ m.

542 **(i)** Percentage of human DRG neurons that were responsive to the indicated tested

543 compounds measured as in **(h)**.

544 **(j)** Venn diagram of the cultured human DRG neurons that were activated by the

545 indicated tested compounds. Green represents DCA responded neurons; Heavy gray

546 represents capsaicin responded neurons; light gray represents histamine responded

547 neurons.

548

549 **Fig. 5 Bile acids and MRGPRX4 specific agonist induce histamine-independent**  
550 **itch in human.**

551 **(a1-a2)** Itch evoked by a double-blind intradermal injection of DCA and nateglinide  
552 (Nat) in human subjects. (25  $\mu$ l for each injection) **(a1)** Time course of the  
553 perceived itch intensity (n = 18-32). The traces are plotted with the standard error of  
554 the mean (s.e.m.) at the peak of each trace. The descriptions of the itch intensity are  
555 shown on the right. The injection sites on the subject's forearm are indicated. X4,  
556 MRGPRX4 **(a2)** Summary of the area-under-the-curve (AUC) of the itch intensity  
557 traces shown in **(a1)**.

558 **(b1-b2)** Itch evoked by the indicated doses of DCA (25  $\mu$ l for each injection, n = 8-14).  
559 The linear regression analysis of concentration versus the AUC is showed as a red  
560 line.

561 **(c1-c2)** Itch evoked by CDCA, CA, TCDCA, and LCA (25  $\mu$ l for each injection, n =  
562 10-31). The vehicle data (Veh) is reproduced from **(a1)**.

563 **(d1-d2)** DCA-evoked itch is not inhibited by antihistamine (Anti-His). **(d1)** Time course  
564 of itch intensity evoked by an intradermal injection of DCA or histamine (His) following  
565 antihistamine or placebo pretreatment (25  $\mu$ l for each injection, n = 12-14). Each pair  
566 of dots connected by a gray line represents an individual subject.

567 Student's *t*-test, \*\* $p < 0.01$ , \*\*\* $p < 0.001$ , and n.s. = not significant ( $p > 0.05$ ).

568

569 **Fig. 6 TGR5 does not serve as an itch receptor in human**

570 **(a1-a2)** Intradermal injection of a non-bile acid TGR5 agonist compound 15 (C15)  
571 does not induce itch in human. **(a1)** Time course of the perceived intensity of itch  
572 evoked by DCA and vehicle are reproduced from **Fig. 5a1**, and the itch evoked by  
573 C15 is from 19 subjects. The equivalent concentration (equiv. conc.) of DCA and C15  
574 means the fold of concentration to the  $EC_{50}$  of activating human TGR5. **(a2)** The  
575 quantification results of area under curve (AUC) of itch intensity shown in **(a1)** (mean  
576  $\pm$  s.e.m.). Veh, vehicle. Student's *t*-test, \*\*\* $p < 0.001$ , and n.s. not significant ( $p >$   
577 0.05).

578 **(b-c)** The activation of human MRGPRX4 **(b)** or human TGR5 **(c)** by DCA (red),  
579 compound 15 (C15, green) and nateglinide in MRGPRX4- or TGR5-expressing  
580 HEK293T cells detected by FLIPR and luciferase assay respectively..

581 **(d)** The relationship between the evoked itch and the relative potency to activate  
582 human MRGPRX4 or human TGR5 by the specific agonists of these two receptors.  
583 The Y-axis shows the relative activation of certain compound to the receptor,  
584 representing the logarithm of (maximal response/ $EC_{50}$ ). The X-axis shows the  
585 human itch intensity, representing the AUC of itch evoked by certain compound.  
586 Statistic test was performed between the itch intensity of compound 15 and vehicle,  
587 or between the itch intensity of nateglinide and vehicle. Nat, nateglinide; C15,  
588 compound 15; Veh, vehicle. Student's *t*-test, \*\* $p < 0.01$ , and n.s. not significant ( $p >$   
589 0.05).

590 **(e)** *In situ* hybridization (ISH) of TGR5 in human DRG sections. **(left)** The diagram  
591 depicting the morphology of DRG neurons and surrounding satellite glial cells.

592 **(middle and right)** TGR5 was highly expressed in satellite glial cells (indicated by  
593 arrows) but not DRG neurons in human DRG. Scale bar, 50  $\mu\text{m}$

594 **(f)** *In situ* hybridization of TGR5 in mouse DRG sections. TGR5 was highly expressed  
595 in DRG neurons (indicated by arrow heads) in mouse DRG. Scale bar, 50  $\mu\text{m}$

596 **(g-h)** Immunohistochemistry (IHC) of human and mouse DRG sections. **(g)** In human  
597 DRG, TGR5 was expressed in satellite glial cells (indicated by arrows) but not in  
598 neurons (marked by NeuN, indicated by arrow heads). **(h)** In mouse DRG, TGR5 was  
599 expressed in neurons (marked by NeuN, indicated by arrow heads). Scale bar, 50  $\mu\text{m}$   
600 m.

601 **(i)** Quantification of the percentage of TGR5+ neurons (over NeuN+ neurons) in  
602 human and mouse DRG (immunohistochemistry). Chi-square test, \*\* $p < 0.01$ .

603

604 **Fig. 7 Elevated bile acids are correlated with the occurrence of itch among**  
605 **patients with liver disease and are sufficient to activate MRGPRX4.**

606 **(a-b)** Summary of individual bile acid levels **(a)** and total bile acid levels **(b)**, the sum of  
607 the 12 bile acids shown in **a)** in itchy patients with liver diseases (Liver\_itch,  $n = 27$ ),  
608 non-itchy patients liver diseases, (Liver\_non-itch,  $n = 36$ ), and itchy patients with  
609 dermatic diseases (Skin\_itch,  $n = 8$ ). The plasma bile acid levels were measured  
610 using HPLC-MS/MS (inset).

611 **(c-d)** Summary of individual bile acid levels **(c)** and total bile acid levels **(d)**, the sum of  
612 the 12 bile acids shown in **c)** in 13 patients with liver diseases during itch and after  
613 itch relief. The inset shows the separation of standard bile acids by HPLC-MS/MS.

614 **(e-f)** Left,  $\text{Ca}^{2+}$  responses in MRGPRX4-expressing HEK293T cells induced by  
615 application of a mixture of artificial bile acids derived from itchy patients with liver  
616 diseases and healthy subjects. The  $\text{Ca}^{2+}$  signal was measured using Fluo-8 and was  
617 normalized to the signal measured using the 1x liver\_itch mix. The summary data are  
618 shown in **(f)**;  $n = 50$  cells each.

619 **(g)** Proposed model depicting the mechanism underlying itch in patients with liver  
620 diseases. In itchy patients, accumulated bile acids reach the skin via the circulatory  
621 system, where they activate nerve fibers in a subset of MRGPRX4-expressing DRG  
622 neurons. These activated neurons relay the itch signal to the spinal cord and higher  
623 brain centers, eliciting the sensation of itch.

624 Student's *t*-test, \* $p < 0.05$ , \*\* $p < 0.01$ , \*\*\* $p < 0.001$ .

## 625 **Supplementary figures**

626

### 627 **Supplementary Fig. 1 Construct design and surface expression of candidate** 628 **GPCRs in HEK293T cells.**

629 **(a)** Map of the generic GPCR expression vector. The 3' and 5' terminal repeats (TR)  
630 are recognized by the PiggyBac transposase. Myc, Myc tag; Puro<sup>R</sup>,  
631 puromycin-resistance gene.

632 **(b)** Plasma membrane expression of the indicated GPCRs transiently expressed in  
633 HEK293T cells, detected using an anti-Myc antibody. Scale bar, 20  $\mu\text{m}$ .

634

635 **Supplementary Fig. 2 <sup>1</sup>H-NMR analysis of bile acids in fractions F1, F2, F3, F4,**  
636 **and F6**

637 The hydrogen chemical shift of CA, CDCA, DCA, and LCA at carbon 3, 7, 12 were  
638 determined by <sup>1</sup>H-NMR. Note that the active fractions (F2 through F4) contained the  
639 characteristic hydrogen peaks corresponding to these bile acids.

640

641 **Supplementary Fig. 3 Human MRGPRX4, but not human MRGPRX1-3 or mouse**  
642 **and rat Mrgpr family members, are activated by bile acids.**

643 (a) Phylogenetic analysis of mouse (Mm, green), rat (Rn, blue), rhesus monkey (Rh,  
644 black), and human (Hs, red) Mas-related GPCR (mrg) family members. Amino acid  
645 sequence similarity compared to Hs. MRGPRX4 is shown in the parenthesis.

646 (b-f) Activation of human MRGPRX1-4 by CA, CDCA, DCA, LCA and Nateglinide  
647 (100 μM each, n = 100 cells from two experiments). Human MRGPRX1-4 were stably  
648 expressed in HEK293T cells, and activation was measured using the Ca<sup>2+</sup> indicator  
649 Fluo-8. Responses are normalized to Bam8-22 (20 μM), PAMP9-20 (20 μM), ATP  
650 (50 μM), and DCA (100 μM) for MRGPRX1, MRGPRX2, MRGPRX3, and  
651 MRGPRX4, respectively. The data for MRGPRX4 (e) are reproduced from **Fig. 3f**.

652 (g-h) Mouse and rat Mrgpr family members are not activated by DCA (100 μM, n = 6  
653 cells) or a mixture of DCA and LCA mix (20 μM each, n = 50 cells).

654

655 **Supplementary Fig. 4 The anti-MRGPRX4 antibody has high specificity.**

656 HEK293T cells were transiently transfected with MRGPRX1, MRGPRX2, MRGPRX3,  
657 or MRGPRX4. The anti-MRGPRX4 antibody (Abcam, ab120808, 1:200 dilution)  
658 specifically labeled MRGPRX4-expressing HEK293T cells, but not MRGPRX1-,  
659 MRGPRX2-, or MRGPRX3-expressing cells. Transfected cells were identified by  
660 mCherry fluorescence, and the nuclei were counterstained with DAPI. Scale bar, 50  
661  $\mu\text{m}$ .

662

663 **Supplementary Fig. 5 Expressing MRGPRX4 in cultured rat DRG neurons**  
664 **renders the cells responsive to bile acids.**

665 (a) Top, cultured rat DRG neurons were transfected with the  
666 pPiggyBac-CAG-MRGPRX4-P2A-mCherry plasmid by electroporation. The cells  
667 circled by dashed lines are an MRGPRX4-positive neuron (neuron 2 with red  
668 fluorescence) and an MRGPRX4-negative (neuron 1) neuron. Bottom,  
669 non-transfected cultured rat DRG neurons. A representative neuron (neuron 3) is  
670 circled by a dash line. Scale bar, 50  $\mu\text{m}$ .

671 (b) Representative traces from the cells indicated in (a). DCA and CA: 10  $\mu\text{M}$ ;  
672 capsaicin (Cap): 1  $\mu\text{M}$ ; KCl: 75 mM.

673 (c) Summary of the amplitude and percentage of  $\text{Ca}^{2+}$  signals in response to DCA  
674 and CA. Responsive neurons were defined as exceeding a threshold of 20%  $\Delta\text{F}/\text{F}_0$ .  
675 n = 60-77 neurons per group.

676 **(d)** Summary of the amplitude and percentage of  $\text{Ca}^{2+}$  signals in response to  
677 capsaicin and KCl. Responsive neurons were defined as in **(c)**.  $n = 67$ -95 neurons per  
678 group.

679 Student's *t*-test or two-proportion z-test, \* $p < 0.05$ , \*\* $p < 0.01$ , \*\*\* $p < 0.001$ , and n.s. =  
680 not significant ( $p > 0.05$ ).

681

682 **Supplementary Fig. 6 Cultured human DRG neurons respond to various**  
683 **chemicals.**

684  $\text{Ca}^{2+}$  imaging of human DRG neurons from one human embryo (donor 1) and three  
685 adult donors (donors 2-4).

686 **(a)** Representative bright-field and fluorescence images of cultured human DRG  
687 neurons. Scale bar, 50  $\mu\text{m}$ .

688 **(b)** Representative  $\text{Ca}^{2+}$  traces in response to the indicated test compounds  
689 measured in the cells shown in **(a)**. Veh, vehicle. Compound 15 (C15), CA and DCA:  
690 100  $\mu\text{M}$ ; histamine (His): 50  $\mu\text{M}$ ; capsaicin (Cap): 1  $\mu\text{M}$ ; KCl: 75 mM.

691 **(c)** Summary of the percentage of neurons that responded to the indicated test  
692 compounds (defined as exceeding a threshold of  $> 20\% \Delta F/F_0$ ).

693

694

695

696

697 **Supplementary Fig. 7 Expression of TGR5 in mouse and monkey DRG**



698 (a) Phylogenetic analysis of mouse (Mm.), rat (Rn.), rhesus monkey (Rh,) and human  
699 (Hs,) TGR5. Amino acid sequence similarity compared to Hs. TGR5 is shown in the  
700 parenthesis.

701 (b) The HEK293T cells were transiently transfected with human TGR5 expression  
702 vector (pPiggyBac-TGR5-P2A-mCherry). The anti-TGR5 antibody can specifically  
703 labeled the TGR5-expressing cells identified by the mCherry signal. The nuclei were  
704 counterstained with DAPI. Arrow heads indicate the representative TGR5-expressing  
705 cells. Scale bar, 20  $\mu\text{m}$ .

706 (c) *In situ* hybridization (ISH) of TGR5 in mouse showing the morphology of mouse  
707 DRG and the adjacent spinal cord. Scale bar, 100  $\mu\text{m}$ .

708 (d) *In situ* hybridization of TGR5 in monkey (*Macaca mulatta*) DRG sections. TGR5  
709 was highly expressed in satellite glial cells (indicated by arrows). Scale bar, 50  $\mu\text{m}$

710 (e) Immunohistochemistry (IHC) of monkey DRG sections. TGR5 was expressed in  
711 satellite glial cells (indicated by arrows) but not neurons (marked by NeuN, indicated  
712 by arrow heads). Scale bar, 50  $\mu\text{m}$ .

713

#### 714 **Supplementary Fig. 8 Quantification of bile acids in human plasma**

715 (a) Standard curve of 12 bile acids quantified by HPLC-MS/MS. All the 12 bile acids  
716 show good linear correlation between the MS response and the concentration (0.1-1  
717  $\mu\text{M}$ )

718 (b) Quantification results of 8 bile acids shown in **Fig. 7a**.

719 (c) Quantification results of 8 bile acids shown in **Fig. 7c**.

720 All error bars represent the s.e.m.; student's *t*-test, \**p* < 0.05, and n.s. = not significant  
721 (*p* > 0.05).

722

723 **Supplementary Fig 9. Bilirubin potentiates the activation of MRGPRX4 by bile**  
724 **acids and may contribute to cholestatic itch.**

725 **(a)** Comparison of the activation of MRGPRX4 by DCA, bilirubin and taurine  
726 conjugated bilirubin. Taurine conjugated bilirubin was used in order to mimic the  
727 direct bilirubin under human physiological condition. MRGPRX4 was expressed in  
728 HEK293T cells and the activation was measured by FLIPR assay.

729 **(b)** Bilirubin allosterically modulates the activation of MRGPRX4 by DCA. Different  
730 concentrations of bilirubin was mixed with DCA, and then the activation of MRGPRX4  
731 by these mixes was tested in MRGPRX4-expressing HEK293T cells using FLIPR  
732 assay.

733 **(c)** DCA allosterically modulates the activation of MRGPRX4 by bilirubin, similar to  
734 **(b).**

735 **(d)** Comparison of total bilirubin, direct bilirubin (conjugated) and indirect bilirubin  
736 (unconjugated) level in liver disease patients with itch (Liver\_itch) (n = 30) or without  
737 itch (Liver\_Non-itc) (n = 34), or patients with dermatic itch (Skin\_itc) (n = 6).

738 **(e)** Comparison of total bilirubin, direct bilirubin and indirect bilirubin level in liver  
739 disease patients (n=12) during itch and after itch relief.

740 (f) Correlation between itch intensity and plasma total bile acid, total bilirubin, direct  
741 bilirubin, and indirect bilirubin. The itch intensity was directly reported by patients via a  
742 questionnaire with 0 representing no itch and 10 the highest level of itch.

743 All error bars represent the s.e.m.. (a-c) One-way ANOVA, \* $p < 0.05$ , \*\* $p < 0.01$ , \*\*\* $p$   
744  $< 0.001$ , and n.s. not significant ( $p > 0.05$ ). (d-f) Student's  $t$ -test, \*\* $p < 0.01$ , \*\*\* $p <$   
745  $0.001$ , and n.s. = not significant ( $p > 0.05$ ).

746

747

748

749 **Supplementary Table. 1 Genes that are highly expressed in human DRG**

750

751 **Supplementary Table 2 GPCRs expression profiling in human DRG**

752 Red labeled genes are candidate GPCRs that are highly expressed in human DRG.

753 Blue labeled gene is TGR5.

754

755

756

757 **References**

758 1 Koch, S. C., Acton, D. & Goulding, M. Spinal Circuits for Touch, Pain, and Itch. *Annu Rev*

759 *Physiol* **80**, 189-217, doi:10.1146/annurev-physiol-022516-034303 (2018).

760 2 Tajiri, K. & Shimizu, Y. Recent advances in the management of pruritus in chronic liver

761 diseases. *World J Gastroenterol* **23**, 3418-3426, doi:10.3748/wjg.v23.i19.3418 (2017).

762 3 Thurmond, R. L., Gelfand, E. W. & Dunford, P. J. The role of histamine H1 and H4 receptors in

- 763 allergic inflammation: the search for new antihistamines. *Nat Rev Drug Discov* **7**, 41-53,  
764 doi:10.1038/nrd2465 (2008).
- 765 4 Beuers, U., Kremer, A. E., Bolier, R. & Elferink, R. P. Pruritus in cholestasis: facts and fiction.  
766 *Hepatology* **60**, 399-407, doi:10.1002/hep.26909 (2014).
- 767 5 Imam, M. H., Gossard, A. A., Sinakos, E. & Lindor, K. D. Pathogenesis and management of  
768 pruritus in cholestatic liver disease. *J Gastroenterol Hepatol* **27**, 1150-1158,  
769 doi:10.1111/j.1440-1746.2012.07109.x (2012).
- 770 6 Jenkins, J. K. & Boothby, L. A. Treatment of itching associated with intrahepatic cholestasis of  
771 pregnancy. *Ann Pharmacother* **36**, 1462-1465, doi:10.1345/aph.1A479 (2002).
- 772 7 Kremer, A. E., Oude Elferink, R. P. J. & Beuers, U. Pathophysiology and current management  
773 of pruritus in liver disease. *Clinics and Research in Hepatology and Gastroenterology* **35**,  
774 89-97, doi:10.1016/j.clinre.2010.10.007 (2011).
- 775 8 Alemi, F. *et al.* The TGR5 receptor mediates bile acid-induced itch and analgesia. *J Clin Invest*  
776 **123**, 1513-1530, doi:10.1172/JCI64551 (2013).
- 777 9 Lieu, T. *et al.* The bile acid receptor TGR5 activates the TRPA1 channel to induce itch in mice.  
778 *Gastroenterology* **147**, 1417-1428, doi:10.1053/j.gastro.2014.08.042 (2014).
- 779 10 Cipriani, S. *et al.* Impaired Itching Perception in Murine Models of Cholestasis Is Supported by  
780 Dysregulation of GPBAR1 Signaling. *PLoS One* **10**, e0129866,  
781 doi:10.1371/journal.pone.0129866 (2015).
- 782 11 Meixiong, J. *et al.* Identification of a bilirubin receptor that may mediate a component of  
783 cholestatic itch. *Elife* **8**, doi:10.7554/eLife.44116 (2019).
- 784 12 Belmonte, C. & Viana, F. Molecular and cellular limits to somatosensory specificity. *Mol Pain* **4**,

- 785 14, doi:10.1186/1744-8069-4-14 (2008).
- 786 13 Dong, X. & Dong, X. Peripheral and Central Mechanisms of Itch. *Neuron* **98**, 482-494,  
787 doi:10.1016/j.neuron.2018.03.023 (2018).
- 788 14 Flegel, C., Manteniotis, S., Osthold, S., Hatt, H. & Gisselmann, G. Expression profile of ectopic  
789 olfactory receptors determined by deep sequencing. *PLoS One* **8**, e55368 (2013).
- 790 15 Flegel, C. *et al.* RNA-seq analysis of human trigeminal and dorsal root ganglia with a focus on  
791 chemoreceptors. *PLoS One* **10**, e0128951 (2015).
- 792 16 Liu, Q. *et al.* Sensory neuron-specific GPCR Mrgprs are itch receptors mediating  
793 chloroquine-induced pruritus. *Cell* **139**, 1353-1365, doi:10.1016/j.cell.2009.11.034 (2009).
- 794 17 Liu, Q. *et al.* Mechanisms of itch evoked by beta-alanine. *J Neurosci* **32**, 14532-14537,  
795 doi:10.1523/JNEUROSCI.3509-12.2012 (2012).
- 796 18 Hall, M. P. *et al.* Engineered luciferase reporter from a deep sea shrimp utilizing a novel  
797 imidazopyrazinone substrate. *ACS Chem Biol* **7**, 1848-1857, doi:10.1021/cb3002478 (2012).
- 798 19 Inoue, A. *et al.* TGFalpha shedding assay: an accurate and versatile method for detecting  
799 GPCR activation. *Nat Methods* **9**, 1021-1029, doi:10.1038/nmeth.2172 (2012).
- 800 20 Patapoutian, A. & Reichardt, L. F. Trk receptors: mediators of neurotrophin action. *Curr Opin*  
801 *Neurobiol* **11**, 272-280 (2001).
- 802 21 Han, S. K., Mancino, V. & Simon, M. I. Phospholipase Cbeta 3 mediates the scratching  
803 response activated by the histamine H1 receptor on C-fiber nociceptive neurons. *Neuron* **52**,  
804 691-703, doi:10.1016/j.neuron.2006.09.036 (2006).
- 805 22 Imamachi, N. *et al.* TRPV1-expressing primary afferents generate behavioral responses to  
806 pruritogens via multiple mechanisms. *PNAS* **106**, 11330–11335 (2009).

- 807 23 Wilson, S. R. *et al.* TRPA1 is required for histamine-independent, Mas-related G  
808 protein-coupled receptor-mediated itch. *Nat Neurosci* **14**, 595-602, doi:10.1038/nn.2789  
809 (2011).
- 810 24 Usoskin, D. *et al.* Unbiased classification of sensory neuron types by large-scale single-cell  
811 RNA sequencing. *Nat Neurosci* **18**, 145-153, doi:10.1038/nn.3881 (2015).
- 812 25 Li, C. L. *et al.* Somatosensory neuron types identified by high-coverage single-cell  
813 RNA-sequencing and functional heterogeneity. *Cell Res* **26**, 83-102, doi:10.1038/cr.2015.149  
814 (2016).
- 815 26 Green, B. G. *et al.* Evaluating the 'Labeled Magnitude Scale' for Measuring Sensations of  
816 Taste and Smell. *Chemical Senses* **21**, 323-334 (1996).
- 817 27 Kroeze, W. K. *et al.* PRESTO-Tango as an open-source resource for interrogation of the  
818 druggable human GPCRome. *Nat Struct Mol Biol* **22**, 362-369, doi:10.1038/nsmb.3014 (2015).
- 819 28 J. KIRBY, K. W. H., J. L. BURTON. Pruritic Effect of Bile Salts. *British Medical Journal* **4**,  
820 693-695 (1974).
- 821 29 Varadi, D. P. Pruritus Induced by Crude Bile and Purified Bile Acids. *Arch Dermatol* **109**  
822 (1974).
- 823 30 Hogenauer, K. *et al.* G-protein-coupled bile acid receptor 1 (GPBAR1, TGR5) agonists reduce  
824 the production of proinflammatory cytokines and stabilize the alternative macrophage  
825 phenotype. *J Med Chem* **57**, 10343-10354, doi:10.1021/jm501052c (2014).
- 826 31 Neale, G., Lewis, B., Weaver, V. & Panveliwalla, D. Serum bile acids in liver disease. *Gut* **12**,  
827 145-152 (1971).
- 828 32 Freedman, M. R., Holzbach, R. T. & Ferguson, D. R. Pruritus in cholestasis no direct causative

- 829 role for bile acid retention. *The American Journal of Medicine* **70**, 1011-1016 (1981).
- 830 33 Bartholomew, T. C., Summerfield, J. A., Billing, B. H., Lawson, A. M. & Setchell, K. D. Bile acid  
831 profiles of human serum and skin interstitial fluid and their relationship to pruritus studied by  
832 gas chromatography-mass spectrometry. *Clin Sci (Lond)* **63**, 65-73 (1982).
- 833 34 Leslie Schoenfield & Sjoval, J. Bile acids on the skin of patients with pruritus hepatobiliary  
834 disease. *Nature* **January 7**, 93-94 (1967).
- 835 35 Xiang, X. *et al.* High performance liquid chromatography-tandem mass spectrometry for the  
836 determination of bile acid concentrations in human plasma. *J Chromatogr B Analyt Technol*  
837 *Biomed Life Sci* **878**, 51-60, doi:10.1016/j.jchromb.2009.11.019 (2010).
- 838 36 Jenkins, H. H., Spencer, E. D., Weissgerber, A. J., Osborne, L. A. & Pellegrini, J. E.  
839 Correlating an 11-point verbal numeric rating scale to a 4-point verbal rating scale in the  
840 measurement of pruritus. *J Perianesth Nurs* **24**, 152-155, doi:10.1016/j.jopan.2009.01.010  
841 (2009).
- 842 37 Lek, M. *et al.* Analysis of protein-coding genetic variation in 60,706 humans. *Nature* **536**,  
843 285-291, doi:10.1038/nature19057 (2016).
- 844 38 Hill, R. NK1 (substance P) receptor antagonists--why are they not analgesic in humans?  
845 *Trends Pharmacol Sci* **21**, 244-246 (2000).
- 846 39 Mogil, J. S. Animal models of pain: progress and challenges. *Nat Rev Neurosci* **10**, 283-294,  
847 doi:10.1038/nrn2606 (2009).
- 848 40 Hug, A. & Weidner, N. From bench to bedside to cure spinal cord injury: lost in translation? *Int*  
849 *Rev Neurobiol* **106**, 173-196, doi:10.1016/B978-0-12-407178-0.00008-9 (2012).
- 850 41 Taneja, A., Di Iorio, V. L., Danhof, M. & Della Pasqua, O. Translation of drug effects from

851 experimental models of neuropathic pain and analgesia to humans. *Drug Discov Today* **17**,

852 837-849, doi:10.1016/j.drudis.2012.02.010 (2012).

853 42 Geenes, V. & Williamson, C. Intrahepatic cholestasis of pregnancy. *World J Gastroenterol* **15**,

854 2049-2066 (2009).

855 43 Yusa, K., Zhou, L., Li, M. A., Bradley, A. & Craig, N. L. A hyperactive piggyBac transposase for

856 mammalian applications. *Proc Natl Acad Sci U S A* **108**, 1531-1536,

857 doi:10.1073/pnas.1008322108 (2011).

858



## 859 **MATERIALS AND METHODS**

### 860 ***Analysis of GPCRs expressed in human DRG neurons***

861 The expression profile of all genes in hDRG neurons was compared to human  
862 reference tissues, including trigeminal ganglia, brain, colon, liver, lung, muscle, and  
863 testis<sup>14,15</sup>. To identify DRG-enriched GPCRs, we using the following formula: [(the  
864 expression level of a given gene in the DRG)/(the total expression level of that gene  
865 in all tissues)]; a value  $\geq 0.5$  was used to define DRG-enriched genes. The expression  
866 level of a gene refers to the number of fragments per kilobase of exon per million  
867 fragments mapped (FPKM) in the tissue transcriptome.

868

### 869 ***Bovine tissue extracts***

870 Fresh bovine heart, brain, kidney, spleen, and liver tissues (40 g each) were  
871 dissected and then boiled for 5 min in 200 ml water. Acetic acid and HCl were then  
872 added to a final concentration of 1 M and 20 mM, respectively, and the mixture was  
873 homogenized thoroughly and then centrifuged at 11,000 rpm for 30 min. The  
874 supernatant was collected and concentrated to a volume of 40 ml using a rotary  
875 evaporator. Acetone (80 ml) was then added to the concentrated solution, and the  
876 new solution was again centrifuged at 11,000 rpm for 30 minutes. The supernatant  
877 was collected using a rotary evaporator and freeze-dried in a vacuum. The final  
878 product was weighed, and equal amounts of each extract were used to test for  
879 activity.

880

881 ***Generation of stable GPCR-expressing cell lines***

882 Stable cell lines expressing orphan GPCRs were generated using the PiggyBac  
883 Transposon System. In brief, each orphan GPCR was subcloned into the PiggyBac  
884 Transposon vector and co-transfected with the hyperactive PiggyBac transposase<sup>43</sup>  
885 into the HEK293T-based TGF $\alpha$  shedding reporter cell line<sup>19</sup> using polyethylenimine  
886 (PEI). Receptor-expressing cells were selected and maintained in DMEM containing  
887 10% fetal bovine serum (FBS), 1  $\mu$ g/ml puromycin, 100 U penicillin, and 100  $\mu$ g/ml  
888 streptomycin in a humidified atmosphere at 37°C containing 5% CO<sub>2</sub>.

889

890 ***TGF $\alpha$  shedding assay***

891 Cultured cells expressing orphan GPCRs were rinsed once with Mg<sup>2+</sup>-free and  
892 Ca<sup>2+</sup>-free phosphate-buffered saline (PBS) and then detached with 0.05% (w/v)  
893 trypsin. The cell suspension was transferred to a 15-ml tube and centrifuged at 190xg  
894 for 5 min. The supernatant was discarded, and the cell pellet was suspended in 10 ml  
895 PBS and incubated for 15 min at room temperature (RT). The cells were  
896 re-centrifuged and suspended in 4 ml HBSS (Hanks' balanced salt solution)  
897 containing 5 mM HEPES (pH 7.4). The suspended cells were then seeded in a  
898 96-well plate at 40,000-50,000 cells per well and placed in a 37°C incubator in 5%  
899 CO<sub>2</sub> for 30 min. A 10x stock solution of each drug was prepared in assay buffer  
900 (HBSS containing 5 mM HEPES, pH 7.4), and 10  $\mu$ l of 10x stock solution was added  
901 to each well. The plate was then placed in the incubator for 2 hr, after which alkaline  
902 phosphatase (AP) activity was measured in the conditioned media and cells.

903

904 ***FLIPR assay***

905 HEK293T cells stably expressing human MRGPRX4 were seeded in 96-well plates at  
906 a density of ~50,000 cells per well. The following day, the cells were loaded with  
907 Fluo-8 (Screen Quest Fluo-8 No-Wash Calcium Assay Kit, AAT Bioquest, Cat. No.  
908 36316) for 2 hr, and test compounds were added to the wells. The Fluo-8 signal was  
909 measured using the FLIPR TETRA system (PerkinElmer).

910

911 ***Luciferase assay***

912 We generated a luciferase reporter plasmid that encodes secreted NanoLuc under  
913 the control of a cAMP response element (CRE) and a minimal promoter. The  
914 hygromycin-resistance gene and EBFP driven by the SV40 promoter in the reporter  
915 plasmid were used to generate stable cell lines. HEK293T cells were transfected with  
916 this plasmid, and a stable cell line was generated by selecting with hygromycin.

917 This stable reporter cell line was then transfected with various GPCRs and used  
918 to monitor the activation of these receptors. In brief, the cells were seeded in 96-well  
919 plates; the next day, the culture medium was replaced, and compounds were added  
920 to the wells; forskolin (10  $\mu$ M final concentration) and 0.01% DMSO (v/v) were used  
921 as positive and negative controls, respectively. The plates were incubated at 37°C in  
922 5% CO<sub>2</sub> for 24 hr, after which a 10- $\mu$ l aliquot of cell culture medium was removed from  
923 each well and combined with 40  $\mu$ l culture medium plus 50  $\mu$ l assay buffer (containing  
924 20  $\mu$ M of the luciferase substrate coelenterazine); after 5 min incubation,

925 luminescence was measured using an EnVision plate reader (PerkinElmer).

926

### 927 ***Fractionation of bile acid components***

928 A commercially available bovine bile acid powder (126.6 mg) was loaded in a silica  
929 gel column (DCM:MeOH = 10:1). The smaller fractions were combined to form six  
930 larger fractions (F1 through F6) based on analytical thin-layer chromatography  
931 performed using 0.25-mm silica gel 60-F plates. Flash chromatography was  
932 performed using 200–400 mesh silica gel.

933

### 934 ***MS and NMR***

935 High-resolution mass spectrometry was performed at the Peking University Mass  
936 Spectrometry Laboratory using a Bruker Fourier Transform Ion Cyclotron Resonance  
937 Mass Spectrometer Solarix XR. <sup>1</sup>H-NMR spectra were recorded on a Bruker  
938 400-MHz spectrometer at ambient temperature with CDCl<sub>3</sub> as the solvent.

939

### 940 ***Immunostaining and flow cytometry analysis***

941 Suspended live HEK 293 cells stably expressing the point-mutated MRGPRX4 were  
942 washed in washing buffer (1X PBS solution, mixed with 5% fetal bovine serum (FBS))  
943 for 3 times. Then cells were incubated with primary antibody (Sigma-Aldrich Cat. No.  
944 C3956, 1:25 dilution) for 30 minutes, and secondary antibody (AAT Bioquest iFluoro™  
945 Alexa 488 goat antirabbit IgG Cat. No. 1060423, 1:50 dilution) for 1 hour. Cells were  
946 washed for two times after each antibody treatment. Next, cells were resuspended

947 with 300 uL to 500 uL FACS buffer, and fluorescence-activated cell-sorting analysis  
948 was performed, using the BD FACS Calibur Flow cytometer (BD Biosciences), and  
949 the data were analyzed using FlowJo software (Ver. 7.6.1).

950

### 951 ***Cultured human DRG neurons***

952 Collection of DRG tissue from adult humans was approved by the Committee for  
953 Medical Science Research Ethics, Peking University Third Hospital  
954 (IRB00006761-2015238), and collection from human embryos was approved by the  
955 Reproductive Study Ethics Committee of Peking University Third Hospital  
956 (2012SZ-013 and 2017SZ-043) and Beijing Anzhen Hospital (2014012x). DRG  
957 tissues were obtained from adult patients undergoing surgical excision of a  
958 schwannoma; the tissues were placed immediately in ice-cold DMEM/F12 medium.  
959 The tissues were then cut into pieces <1 mm in size and treated with an enzyme  
960 solution containing 5 mg/ml dispase and 1 mg/ml collagenase at 37°C for 1 hr. After  
961 trituration and centrifugation, the cells were washed in 15% (w/v) bovine serum  
962 albumin (BSA) resuspended in DMEM/F12 containing 10% FBS, plated on glass  
963 coverslips coated with poly-D-lysine and laminin, cultured in an incubator at 37°C,  
964 and used within 24 hr of plating.

965

### 966 ***Culture and electroporation of rodent DRG neurons***

967 Rat DRG tissues were obtained from the thoracic and lumbar vertebrae and placed in  
968 ice-cold DMEM/F12 medium. The tissues were cut into pieces <1 mm in size and

969 then treated with an enzyme solution containing 5 mg/ml dispase and 1 mg/ml  
970 collagenase at 37°C for 1 hr. After trituration and centrifugation, the cells were  
971 washed in 15% BSA, resuspended in DMEM/F12 containing 10% FBS, plated on  
972 glass coverslips coated with poly-D-lysine and laminin, cultured in an incubator at  
973 37°C, and used within 24 hr of plating.

974 Rat DRG neurons were electroporated as follows. After washing the neurons with  
975 15% BSA, the neurons were resuspended in DMEM/F12 and electroporated using a  
976 P3 Primary Cell 4D-Nucleofector X Kit L (cat. no. V4XP-3012, Lonza) in accordance  
977 with the manufacturer's instructions. After electroporation, the neurons were cultured  
978 for 72 hr before use in order to allow the transgenes to express.

979

#### 980 ***Ca<sup>2+</sup> imaging***

981 For Ca<sup>2+</sup> imaging experiments, cells were loaded at 37°C for 1 hr with 10 µg/ml Fluo-8  
982 AM (AAT Bioquest, Inc.) supplemented with 0.01% Pluronic F-127 (w/v; Invitrogen).  
983 Bile acids, bio-mimicked bile acid mixes, and/or various drugs to be tested were  
984 added to the cells in a chamber containing a custom-made 8-channel perfusion valve  
985 control system. Fluorescence images were acquired using a Nikon A1 confocal  
986 microscope.

987

#### 988 ***In situ hybridization and immunostaining***

989 Single colorimetric *in situ* hybridization in hDRG sections was performed as follows.

990 The sections were fixed in freshly prepared 4% paraformaldehyde (PFA) in PBS for

991 20 min at RT, and then washed in fresh-DEPC PBS (1:1000 DEPC was added to 1x  
992 PBS immediately before use) and DEPC-pretreated PBS (1:1000 DEPC in PBS  
993 overnight, followed by autoclaving) for 10 min each. The sections were then  
994 immersed in a DEPC-containing antigen-retrieval solution containing 10 mM citric  
995 acid, 0.05% Tween-20 (pH 6.0) in a 95°C water bath for 20 min, and then cooled at  
996 RT for 30 min. After washing in DEPC-pretreated PBS for 10 min, the sections were  
997 incubated in a Proteinase K solution (25 µg/mL in DEPC-pretreated water) for 20 min  
998 and then washed in fresh-DEPC PBS and DEPC-pretreated PBS (10 min each). The  
999 sections were incubated in freshly prepared acetylation solution containing 0.1 M TEA  
1000 and 0.25% acetic anhydride in DEPC-pretreated water for 10 min at RT, followed by a  
1001 10-min wash in DEPC-pretreated PBS. The prehybridization step was performed in  
1002 probe-free hybridization buffer consisting of 50% formamide, 5x SSC, 0.3 mg/ml  
1003 yeast tRNA, 100 µg/ml heparin, 1x Denhardt's solution, 0.1% Tween-20, 0.1%  
1004 CHAPS, and 5 mM EDTA in RNase-free water at 62°C for 30 min in a humidified  
1005 chamber, followed by an overnight hybridization step in hybridization buffer containing  
1006 5 ng/µl DIG-labeled riboprobes at 62°C in a humidified chamber (under a Parafilm  
1007 coverslip). After the hybridization step, the sections were washed in 0.2x SSC at 68°C  
1008 (once for 15 min and twice for 30 min each), followed by blocking in PBS containing  
1009 0.1% Triton X-100 and 20% horse serum for 1 hr at RT. The sections were then  
1010 stained overnight at 4°C with pre-absorbed AP-conjugated sheep anti-DIG antibody  
1011 (1:1000, Roche, cat. 11093274910) in PBS containing 0.1% Triton X-100 and 20%  
1012 horse serum. The sections were washed 3 times for 10 min each in PBS containing

1013 0.1% Triton X-100, followed by overnight incubation in the dark in AP buffer  
1014 containing 100 mM Tris (pH 9.5), 50 mM MgCl<sub>2</sub>, 100 mM NaCl, 0.1% Tween-20, 5  
1015 mM levamisole, 0.34 mg/ml NBT (Roche cat. no. 11383213001), and 0.17 mg/ml  
1016 BCIP (Roche, cat. no. 1138221001) to allow the color reaction to develop. The  
1017 sections were washed 3 times for 10 min each in PBS, and then fixed for 30 min in 4%  
1018 PFA in PBS. The sections were quickly rinsed 5 times in ddH<sub>2</sub>O, dried at 37°C for 1 hr,  
1019 and dehydrated in xylene (3 times for 2 min each). Finally, the sections were mounted  
1020 under a glass coverslip using Permount (Fisher).

1021 Immunostaining was performed using a rabbit anti-hMRGPRX4 antibody  
1022 obtained (Abcam, cat. no. ab120808). The sections were fixed in freshly prepared 4%  
1023 PFA in PBS for 20 min at RT and then washed in PBS containing 0.1% Triton X-100 3  
1024 times for 10 min each, followed by block in PBS containing 0.1% Triton X-100 and 20%  
1025 horse serum for 1 hour at RT. The sections were then incubated overnight in primary  
1026 antibody at 4°C, washed with PBS containing 0.1% Triton X-100 3 times for 15 min  
1027 each, and incubated with secondary antibody for 1 hour at RT. After washing with  
1028 PBS 3 times for 15 min each, the sections were mounted under glass coverslips and  
1029 Fluoromount-G (Invitrogen).

1030

### 1031 ***RNAscope in situ hybridization***

1032 RNAscope *in situ* hybridization was performed in accordance with the manufacturer's  
1033 instructions (Advanced Cell Diagnostics). In brief, human DRG sections were fixed,  
1034 dehydrated, and treated with protease. The sections were then hybridized with the



1035 respective target probe for 2 hours at 40°C, followed by four-round signal  
1036 amplification. The sections were then mounted under coverslips, sealed with nail  
1037 polish, and stored in the dark at 4°C until imaged.

1038

### 1039 ***Human itch test***

1040 The human itch test studies were approved by the Committee for Protecting Human  
1041 and Animal Subjects at the Department of Psychology, Peking University  
1042 (#2018-05-02). Volunteers were students and faculty members recruited from Peking  
1043 University. All subjects provided written informed consent and were provided with the  
1044 experimental protocol. All injections were performed using an INJEX 30 needle-free  
1045 injection system (INJEX Pharma GmbH, Berlin, Germany). We performed two studies  
1046 as described below.

1047 In the first study (to measure bile acid-induced itch sensation), each tested  
1048 compound was dissolved in physiological saline containing 7% Tween-80  
1049 (Sigma-Aldrich). The injection sites were cleaned with rubbing alcohol, and 25 µl of  
1050 each solution was injected intradermally on the volar surface of each arm. The same  
1051 volume of vehicle (saline containing 7% Tween-80) served as the negative control.  
1052 Itch was defined as the desire to initiate scratching during the experiment, and the  
1053 subjects rate the perceived intensity according the generalized labeled magnitude  
1054 scale (LMS) described by Green et al.<sup>26</sup>

1055 In the second study (to measure the effect of antihistamines on DCA-induced  
1056 itch), two experimental sessions were performed, separated by 2 weeks, with 14 and

1057 12 subjects participating in the first and second sessions, respectively. Approximately  
1058 1.5 g of topical antihistamine cream (doxepin hydrochloride cream, Chongqing  
1059 Huapont Pharm. Co., China) or a placebo cream (cold cream, Eau Thermale Avène,  
1060 Paris, France) was applied 2.5 hr before injection of DCA or histamine  
1061 (Sigma-Aldrich); any unabsorbed cream was removed with alcohol. A 500 µg/25 µl  
1062 solution of DCA was prepared as described above, and a 2.5 µg/25 µl solution of  
1063 histamine was dissolved in saline; 25 µl of the DCA or histamine solution was injected  
1064 into the volar surface of the arm as described above. In the first session, each subject  
1065 received two intradermal injections of DCA (one at the antihistamine-treated site and  
1066 one at the placebo-treated site). In the second session, each subject received two  
1067 intradermal injections of histamine (one at the antihistamine-treated site and one at  
1068 the placebo-treated site). The subjects then rate the itch sensation as described  
1069 above.

1070

#### 1071 ***Quantification of plasma bile acids and bilirubin***

1072 These experiments were approved by the Committee for Biomedical Ethics, Peking  
1073 University First Hospital (2017-R-94). Itch intensity was measured using a self-report  
1074 numerical rating scale (NRS)<sup>36</sup>, and whole blood samples were collected from  
1075 patients with skin diseases and patients with liver diseases. Plasma was obtained by  
1076 centrifuging 2 ml of whole blood at 4°C, 11,000 g for 10 min; 100 µl of each plasma  
1077 sample was then mixed with 400 µl acetonitrile and left to sit at 4°C for 20 min. The  
1078 mixture was centrifuged, and the supernatant was dried in a rotatory evaporator

1079 (45°C under vacuum), and the dried residue was retrieved and dissolved in 60%  
1080 methanol for further analysis.

1081 The bile acid level in plasma samples was measured using HPLC-MS/MS  
1082 (Agilent model LC1260 QQQ 6495). Chromatographic separation was performed in  
1083 an ACQUITY UPLC HSS T3 column (2.1 mm × 100 mm, 1.8 µm; Waters Corp.). The  
1084 mobile phase consisted of solution A (water) and solution B (acetonitrile). The total  
1085 running time was 23 min, and a linear gradient (0.3 ml/min) was applied as follows:  
1086 0-2 min: 10% B - 40% B; 2-18 min: 40% B - 50% B; 18-19 min: 50-100% B; 19-20 min:  
1087 100% B; 20-21 min: 100-10% B; 21-23 min: 10% B. The injection volume was 5 µl,  
1088 and the mobile phase flow rate was 3 ml/min. Deoxycholic-2,2,4,4,11,11-d6 acid  
1089 (Sigma, cat. no. 809675) was used as an internal standard.

1090 Total bilirubin and direct bilirubin values were obtained from the patients' hospital  
1091 blood chemistry reports.

1092

### 1093 ***Statistical analysis***

1094 Summary data are presented as the mean ± SEM. Human subjects were randomly  
1095 assigned to control and experimental groups, and the subjects and investigators were  
1096 double-blinded with respect to the experiment treatments. Data were analyzed using  
1097 the Student's *t*-test, two-proportion *z*-test, Chi-square test or One-way ANOVA and  
1098 differences with a *P*-value of < 0.05 were considered significant.

1099

1100

**Fig. 1** Identification of MRGPRX4 activated by bile extract.

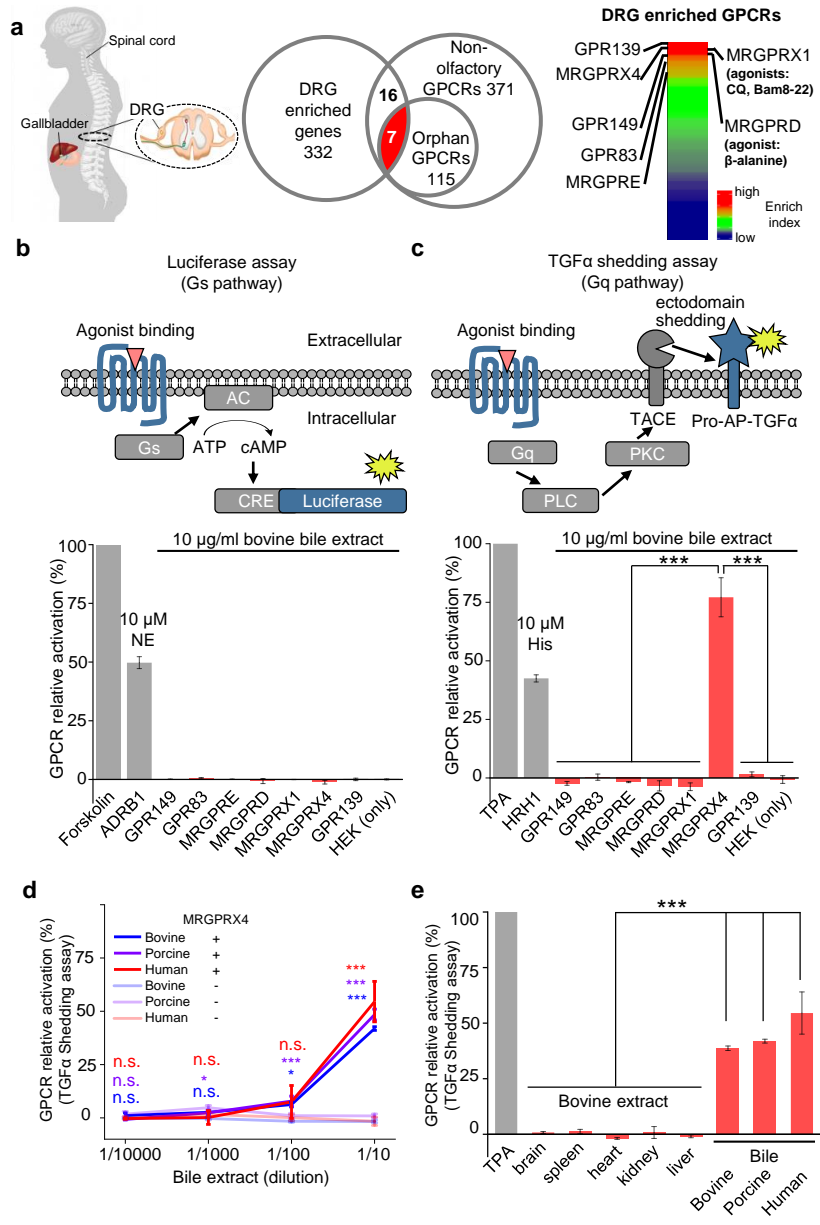


**Fig. 2 Identification of active components that activate MRGPRX4 from bile extract.**

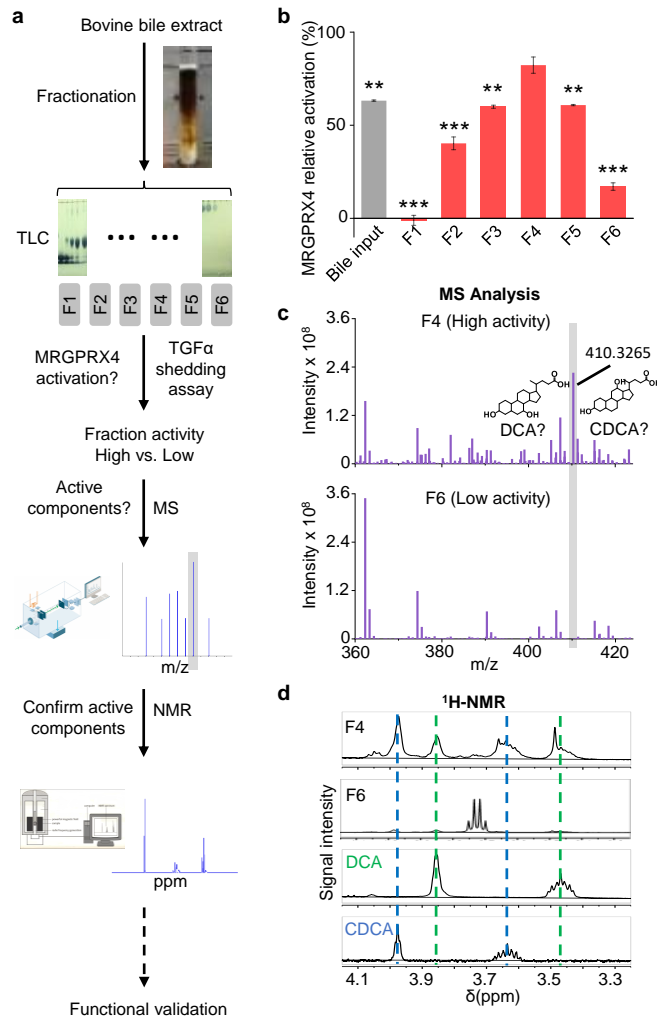


**Fig. 3 Functional characterization and molecular profiling of bile acids as ligands for MRGPRX4**

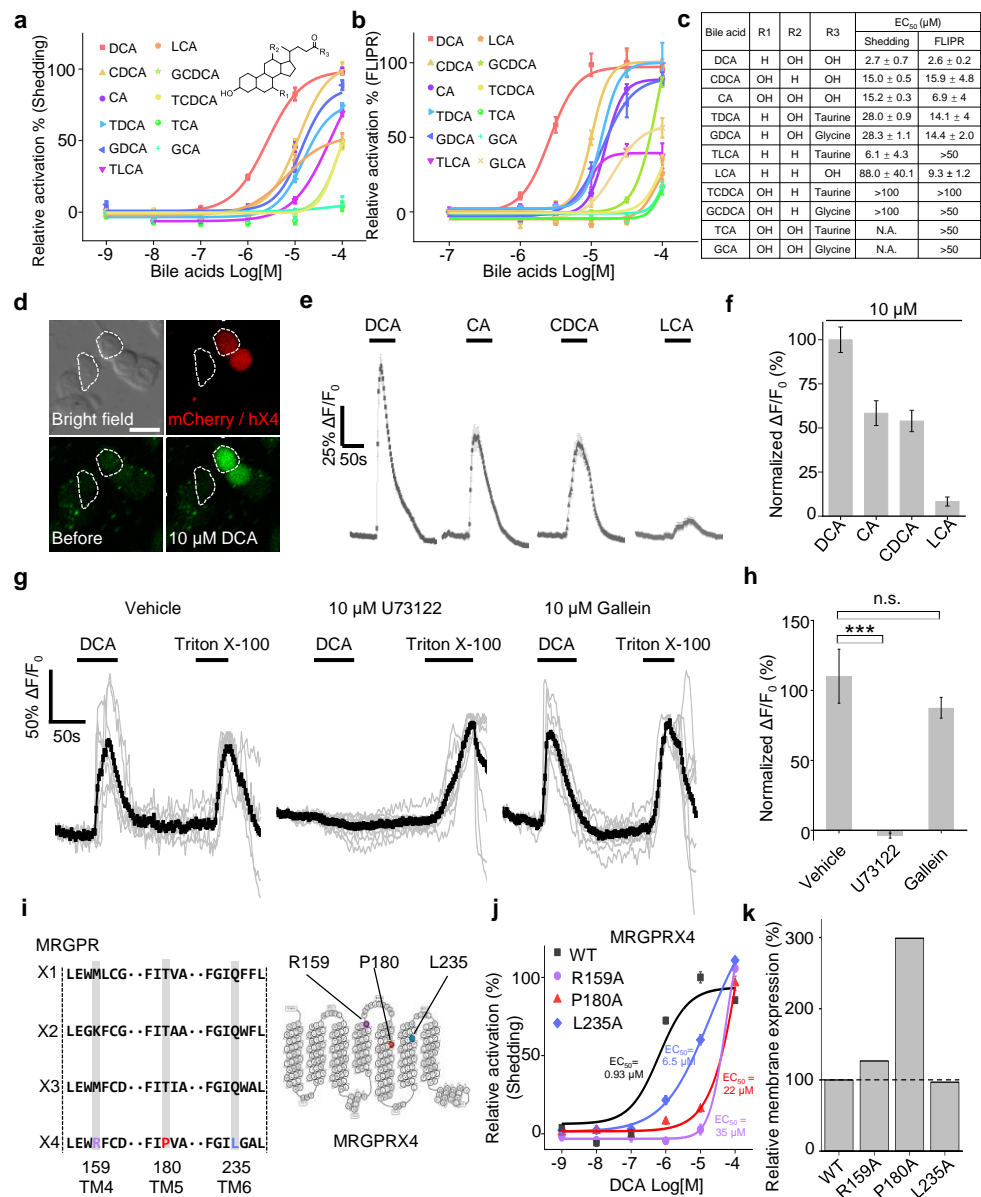


**Fig. 4** A subset of hDRG neurons express MRGPRX4 and respond to bile acids.

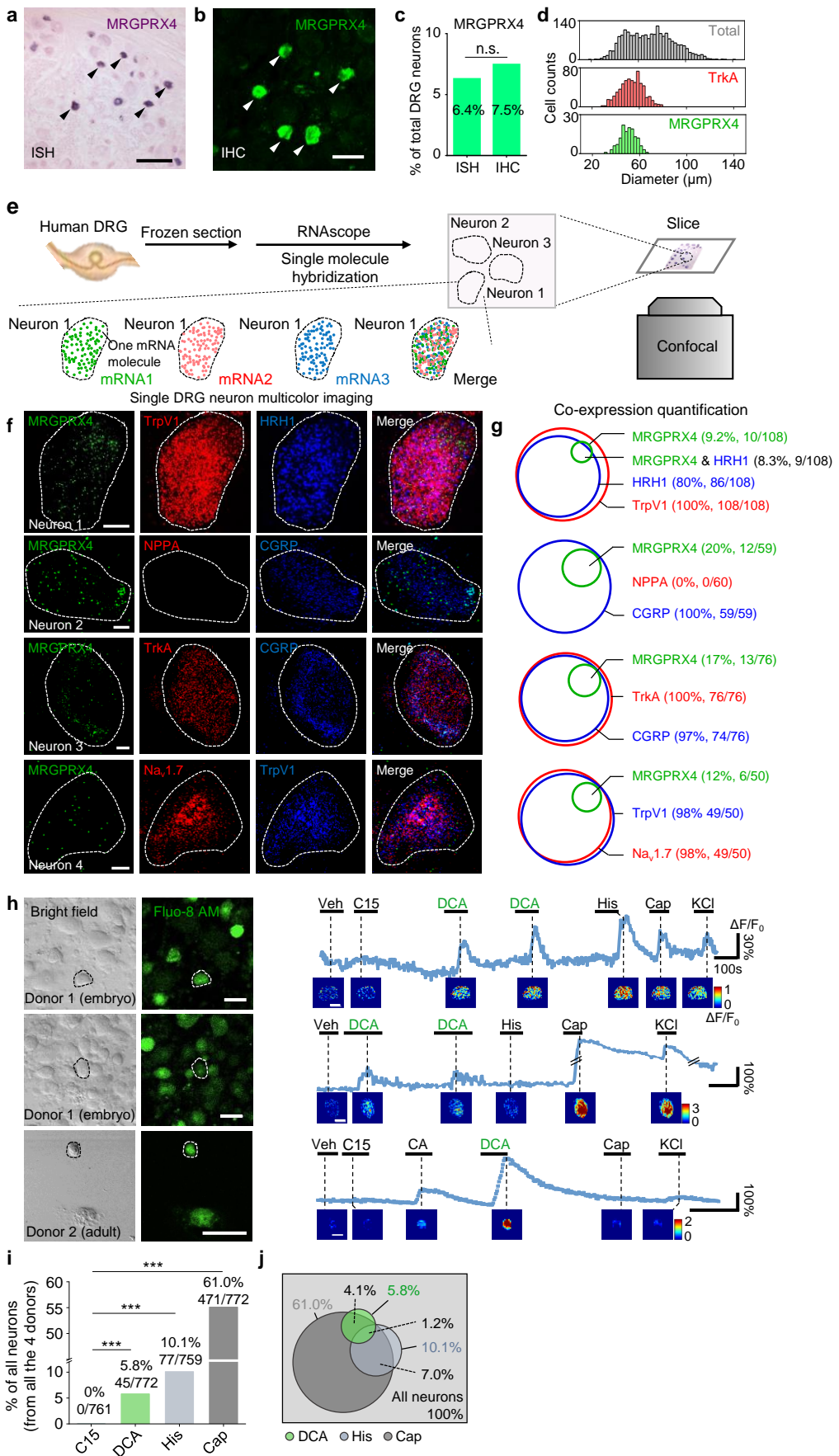


**Fig. 5 Bile acids and MRGPRX4 specific agonist induce histamine-independent itch in human**

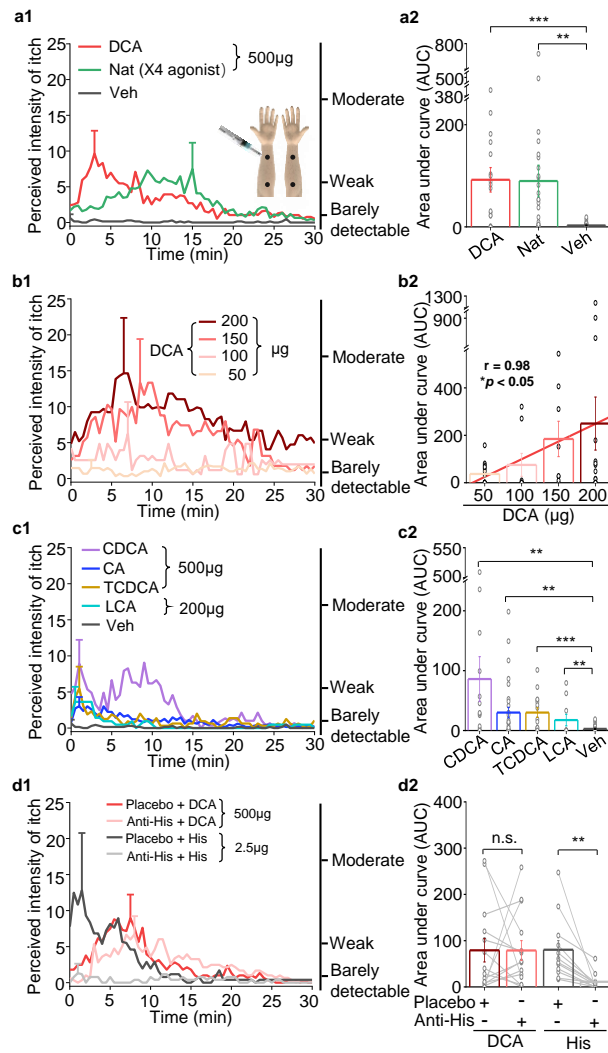
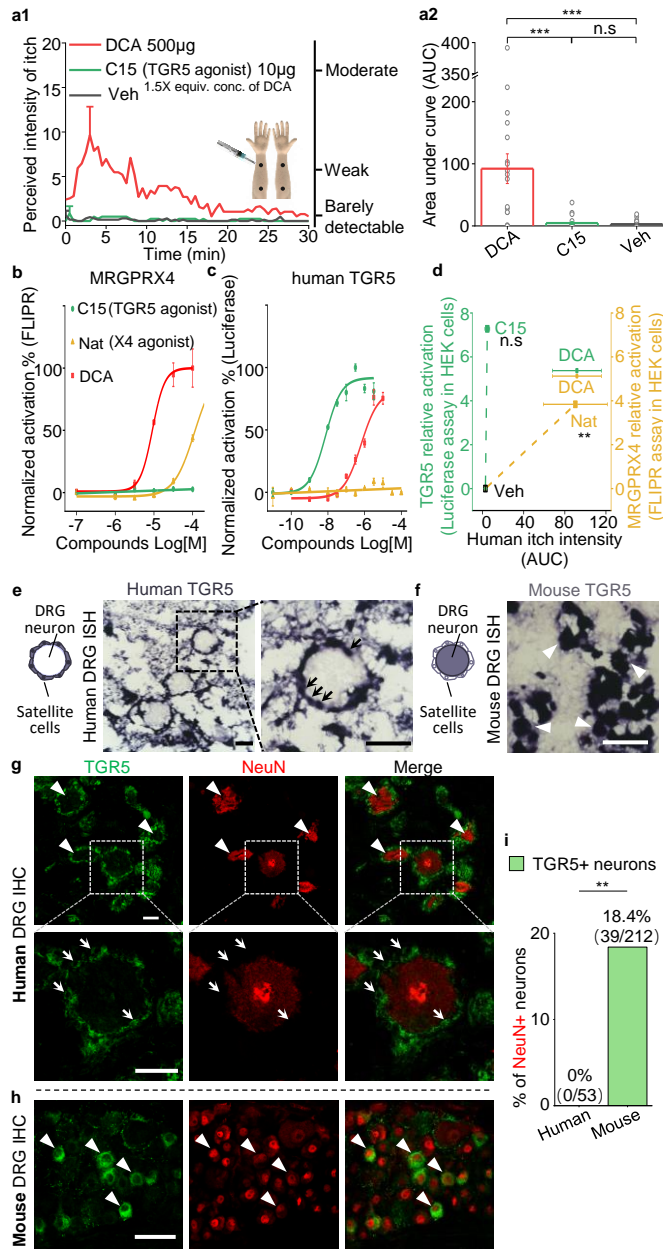
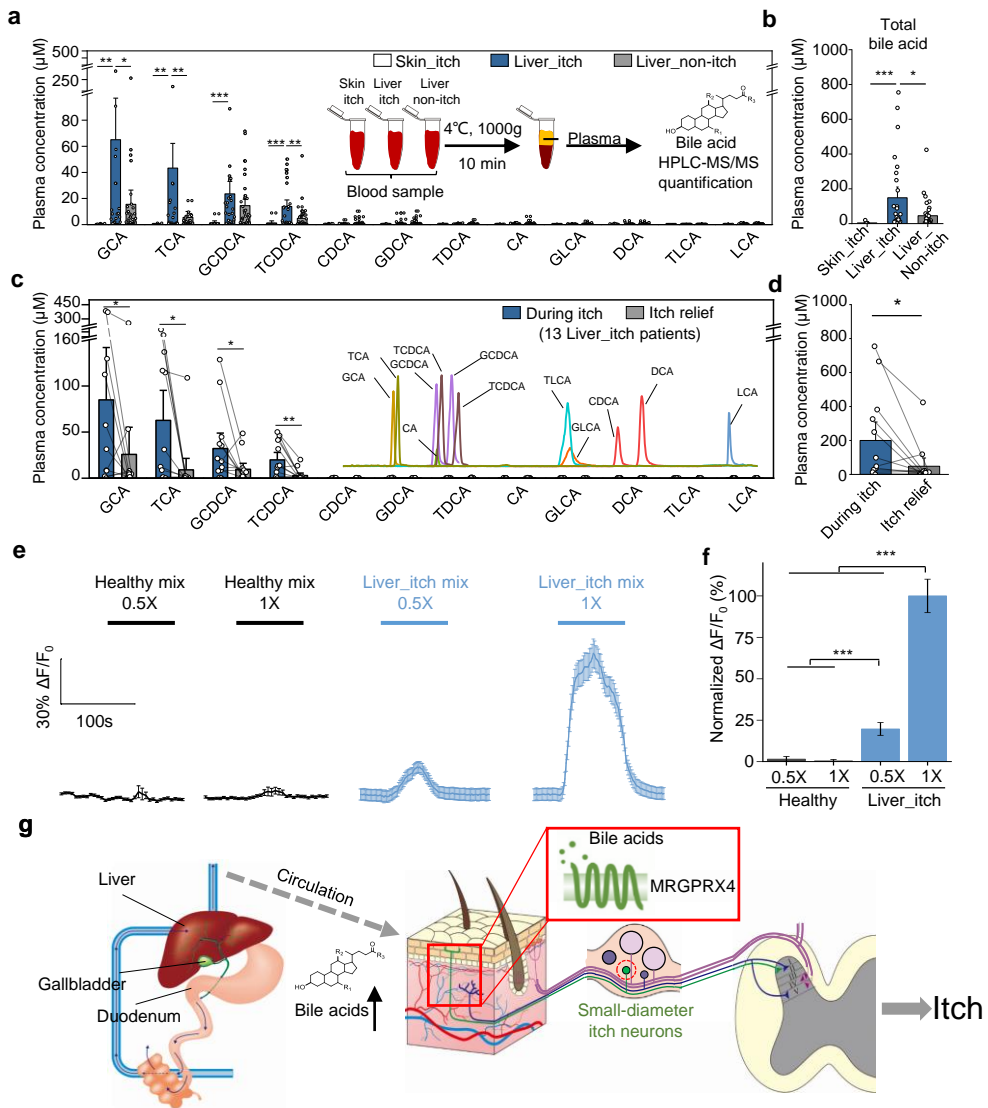




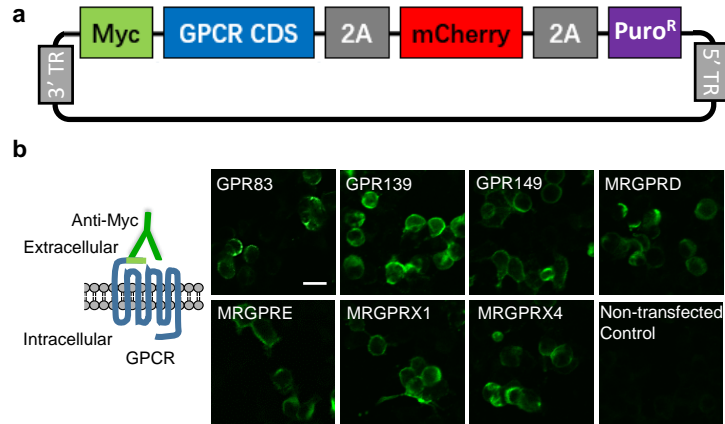
Fig. 6 TGR5 does not serve as an itch receptor in human



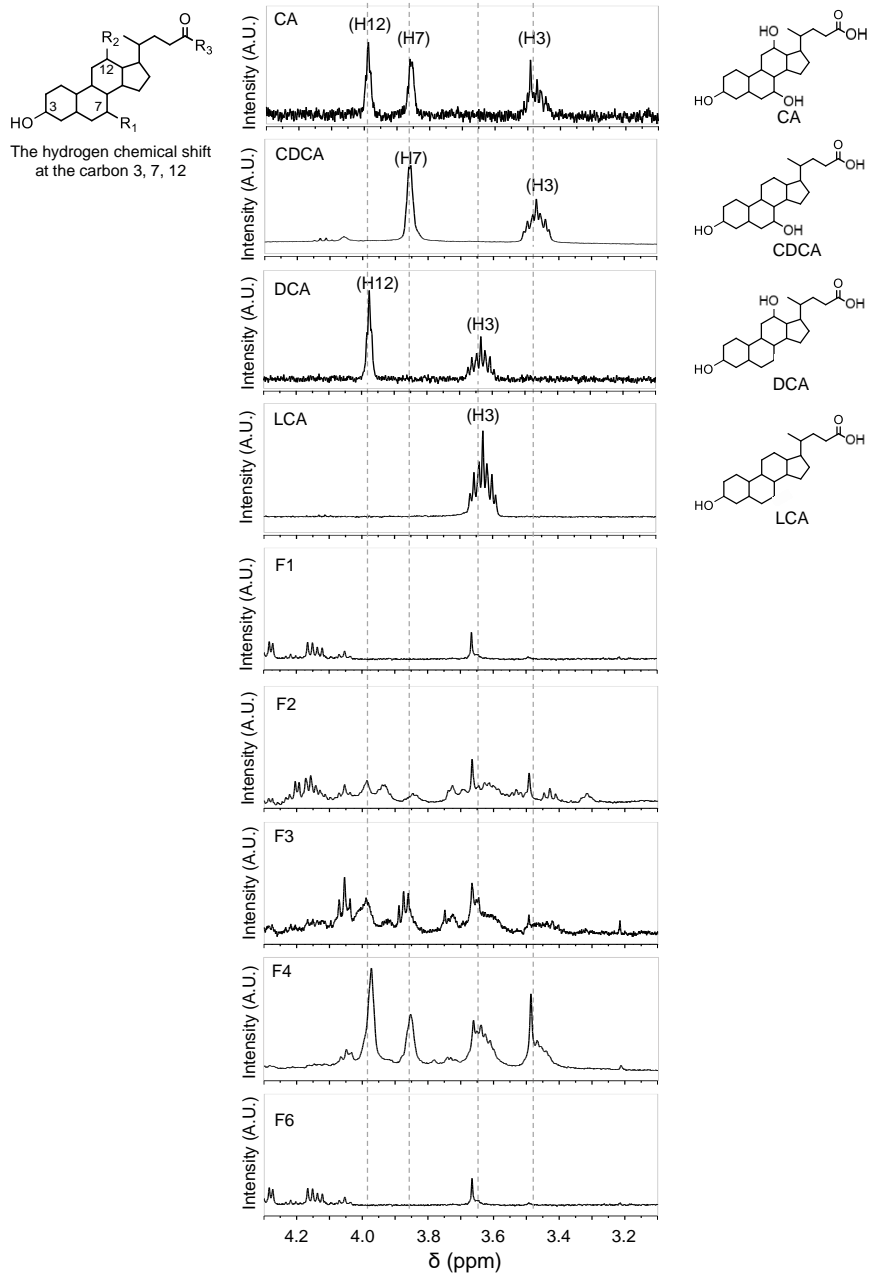
**Fig. 7 Elevated bile acids correlate with the occurrence of itch among liver disease patients and are sufficient to activate MRGPRX4**



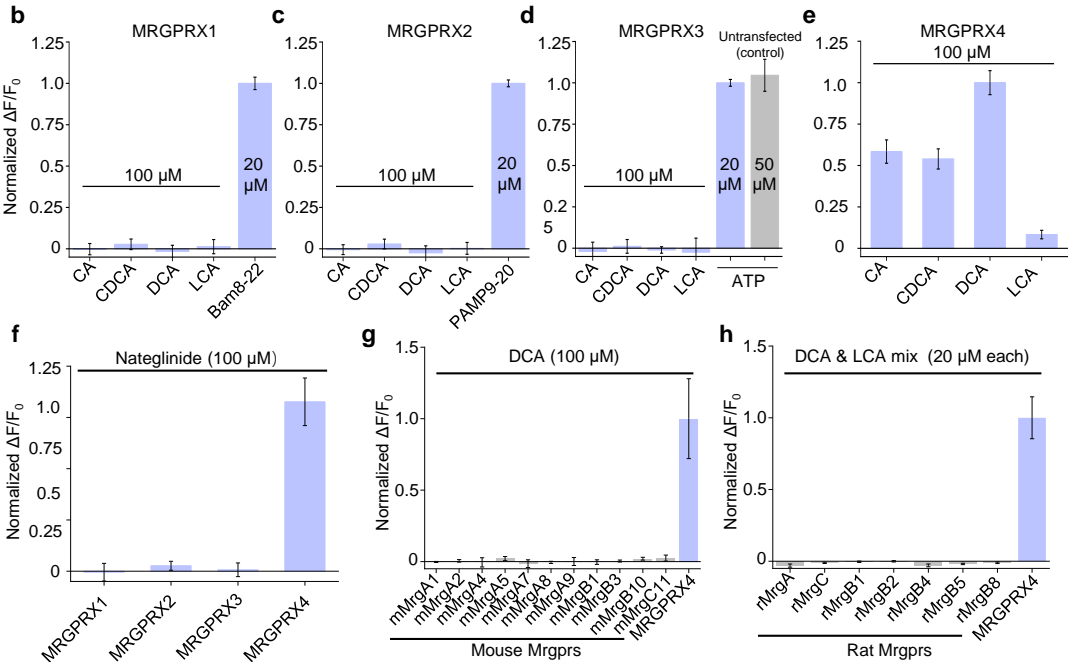
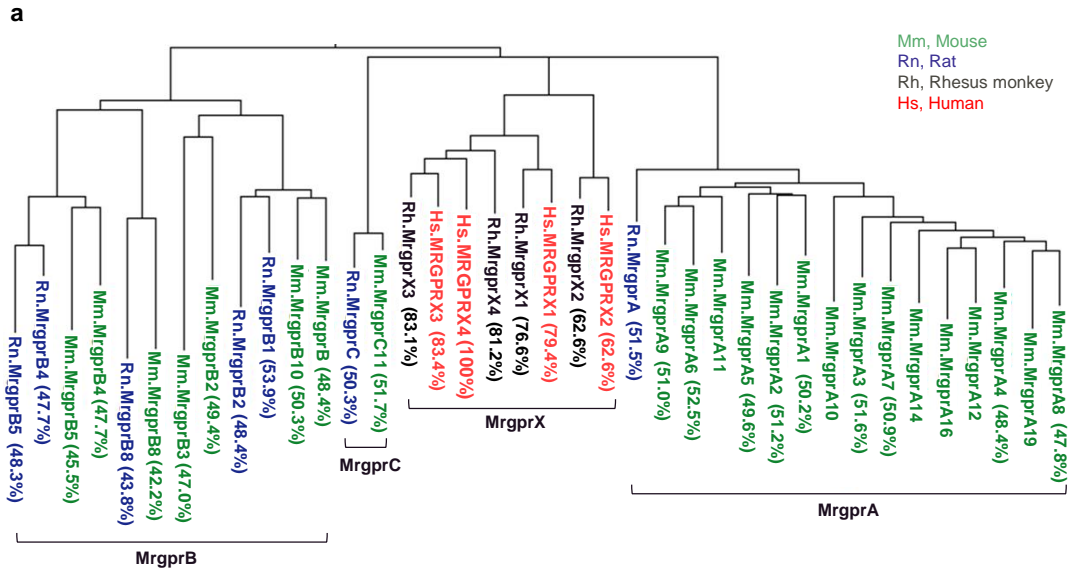
**Supplementary Fig. 1 Construct design and surface expression of candidate GPCRs in HEK293T cells**



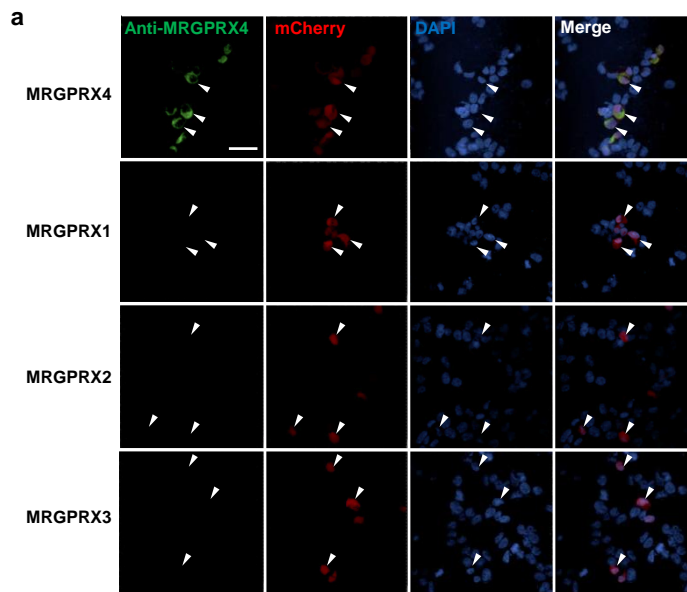
Supplementary Fig. 2  $^1\text{H-NMR}$  analysis of bile acids in fractions F1, F2, F3, F4, and F6



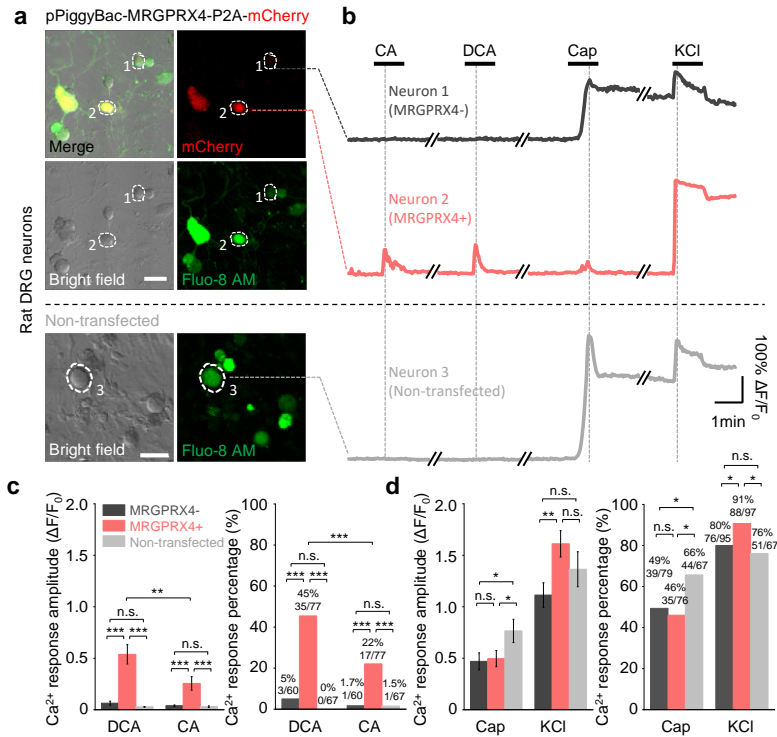
**Supplementary Fig. 3 Human MRGPRX4, but not human MRGPRX1-3 or mouse and rat Mrgpr family members, are activated by bile acids.**



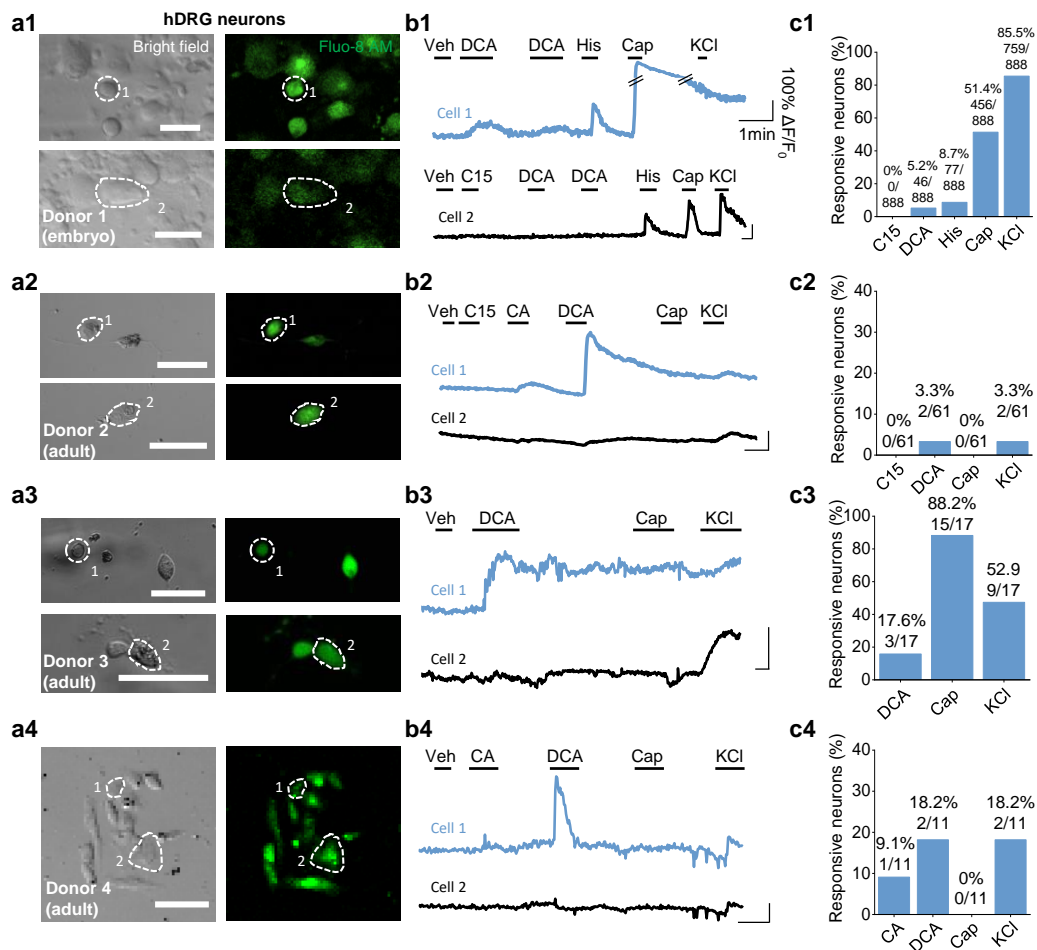
Supplementary Fig. 4 The anti-MRGPRX4 antibody has high specificity.



Supplementary Fig. S5. Expressing MRGPRX4 in cultured rat DRG neurons renders the cells responsive to bile acids.

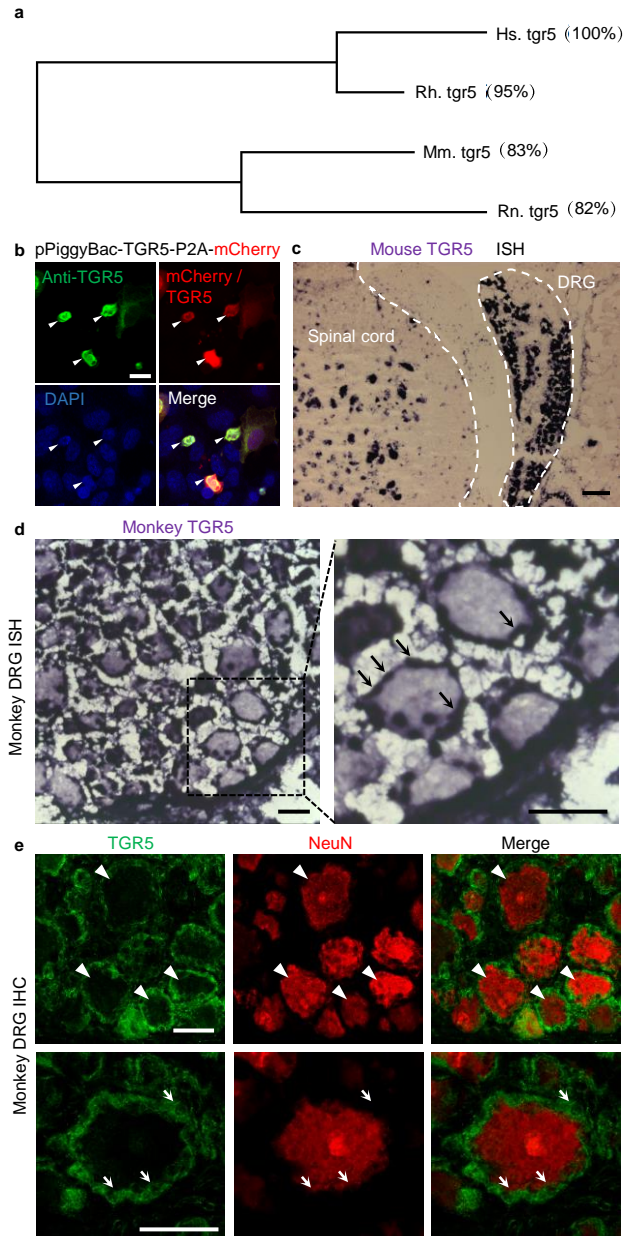


**Supplementary Fig. 6 Cultured human DRG neurons respond to various chemicals**

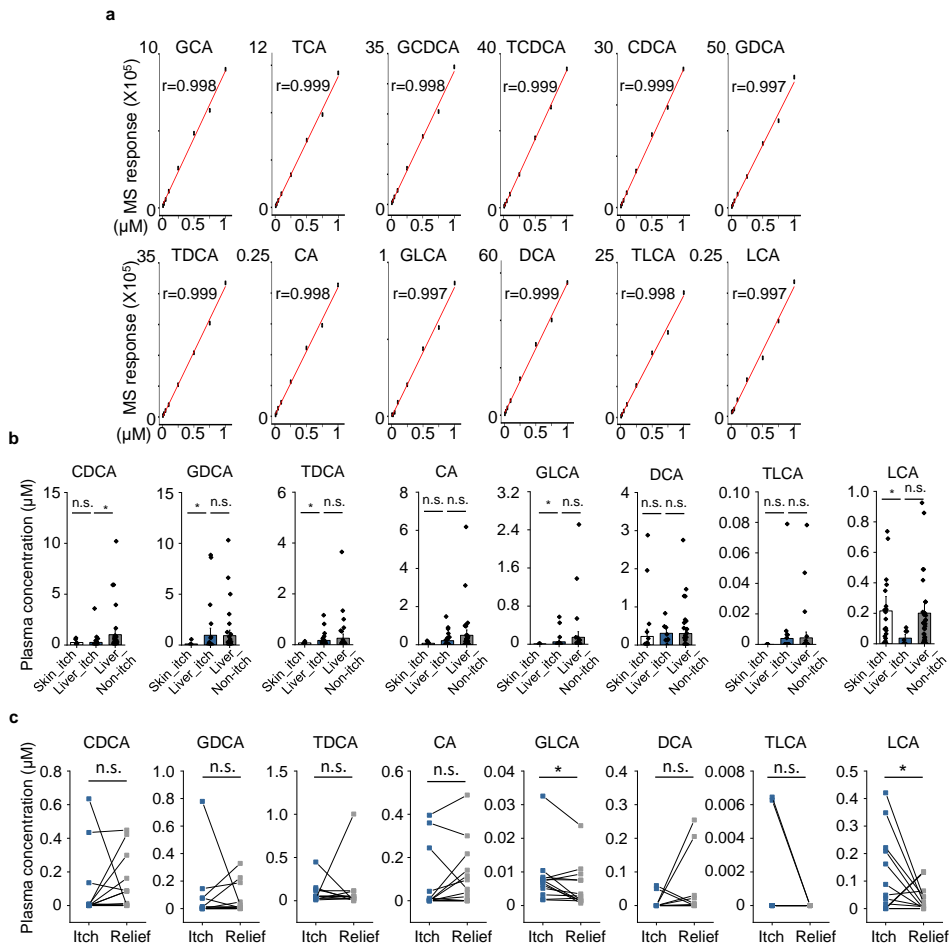




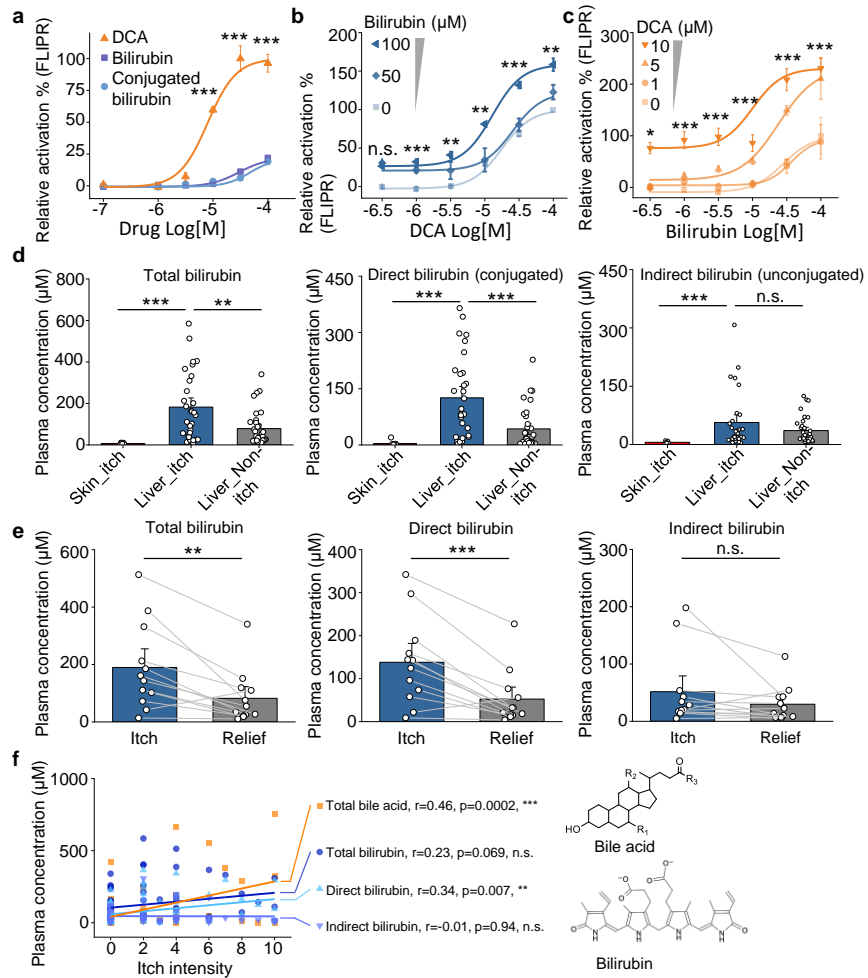
### Supplementary Fig. 7 Expression of TGR5 in mouse and monkey DRG



**Supplementary Fig. 8 Quantification of bile acids in human plasma**



**Supplementary Fig. 9 Bilirubin is an allosteric modulator and potentiates the activation of MRGRPX4 by bile acids and may contribute to cholestatic itch**



Supplementary Table 1 Genes that are highly expressed in human DRG

| Rank | gene       | DRG/All | Rank | gene         | DRG/All | Rank | gene         | DRG/All | Rank | gene         | DRG/All | Rank | gene         | DRG/All |
|------|------------|---------|------|--------------|---------|------|--------------|---------|------|--------------|---------|------|--------------|---------|
| 1    | LOC401164  | 1.0000  | 68   | CCDC140      | 0.6985  | 135  | ANKRD33      | 0.6209  | 202  | GGT8P        | 0.5634  | 269  | MAP7D2       | 0.5279  |
| 2    | LOC645591  | 1.0000  | 69   | PIRT         | 0.6964  | 136  | CHRNA6       | 0.6181  | 203  | CHRM4        | 0.5629  | 270  | LOC100289511 | 0.5278  |
| 3    | MIR1250    | 1.0000  | 70   | VAT1L        | 0.6962  | 137  | EPN3         | 0.6181  | 204  | HOXC6        | 0.5627  | 271  | SLC10A2      | 0.5276  |
| 4    | MIR1914    | 1.0000  | 71   | KRT75        | 0.6956  | 138  | LIPM         | 0.6166  | 205  | LOC100130298 | 0.5623  | 272  | HSPA12A      | 0.5275  |
| 5    | MIR3188    | 1.0000  | 72   | HHLA1        | 0.6948  | 139  | NBPF11       | 0.6150  | 206  | LPAR3        | 0.5623  | 273  | CYP4F24P     | 0.5273  |
| 6    | MIR572     | 1.0000  | 73   | RET          | 0.6899  | 140  | KANK4        | 0.6145  | 207  | FLJ42969     | 0.5611  | 274  | RPL21P28     | 0.5260  |
| 7    | MIR659     | 1.0000  | 74   | G SX1        | 0.6867  | 141  | OR13C5       | 0.6145  | 208  | SLC2A6       | 0.5609  | 275  | B4GALNT1     | 0.5253  |
| 8    | MIR92B     | 1.0000  | 75   | SCN10A       | 0.6867  | 142  | SPDYE2       | 0.6136  | 209  | FGF22        | 0.5606  | 276  | CD1A         | 0.5253  |
| 9    | MSGN1      | 1.0000  | 76   | INSC         | 0.6863  | 143  | PCDHAC2      | 0.6122  | 210  | GRM4         | 0.5602  | 277  | AATK         | 0.5249  |
| 10   | OR10A4     | 1.0000  | 77   | KCNK18       | 0.6858  | 144  | PLD4         | 0.6120  | 211  | FOXO3        | 0.5600  | 278  | RXRG         | 0.5249  |
| 11   | OR2M4      | 1.0000  | 78   | OR2L13       | 0.6853  | 145  | LOC100329108 | 0.6109  | 212  | NKAIN4       | 0.5598  | 279  | CRYBA2       | 0.5228  |
| 12   | OR4H6P     | 1.0000  | 79   | PRPH         | 0.6849  | 146  | TRPV1        | 0.6099  | 213  | LCNL1        | 0.5590  | 280  | KCNA10       | 0.5221  |
| 13   | OR56B2P    | 1.0000  | 80   | LOC441617    | 0.6846  | 147  | HOXD1        | 0.6098  | 214  | TLX2         | 0.5588  | 281  | SYT2         | 0.5214  |
| 14   | P2RX6P     | 1.0000  | 81   | SPTBN5       | 0.6845  | 148  | OR56B4       | 0.6094  | 215  | LOC100130275 | 0.5585  | 282  | TSPAN10      | 0.5208  |
| 15   | OR4N5      | 0.9985  | 82   | SNORD123     | 0.6834  | 149  | TLX3         | 0.6086  | 216  | PDE6H        | 0.5579  | 283  | SNORD116-21  | 0.5202  |
| 16   | OR13C9     | 0.9799  | 83   | CALCB        | 0.6819  | 150  | PROKR2       | 0.6083  | 217  | FOXS1        | 0.5576  | 284  | INSRR        | 0.5201  |
| 17   | SNORD87    | 0.9791  | 84   | TMEM72       | 0.6789  | 151  | KCNG4        | 0.6077  | 218  | CHST8        | 0.5574  | 285  | TUBB2A       | 0.5200  |
| 18   | MIR324     | 0.9375  | 85   | ADAMTS16     | 0.6761  | 152  | NPSR1        | 0.6069  | 219  | F2RL2        | 0.5564  | 286  | C18orf42     | 0.5200  |
| 19   | DYTN       | 0.9317  | 86   | SNORA70B     | 0.6760  | 153  | EGFL8        | 0.6065  | 220  | MIR1247      | 0.5559  | 287  | RESP18       | 0.5187  |
| 20   | CRYGB      | 0.9233  | 87   | MIR630       | 0.6754  | 154  | FZD2         | 0.6061  | 221  | GPR149       | 0.5547  | 288  | PCDHAC1      | 0.5187  |
| 21   | OR2M3      | 0.8983  | 88   | SYT6         | 0.6753  | 155  | SNORD125     | 0.6054  | 222  | EMILIN3      | 0.5540  | 289  | FLJ42875     | 0.5182  |
| 22   | GPR139     | 0.8873  | 89   | OR2T33       | 0.6725  | 156  | TSHB         | 0.6045  | 223  | TMEFF2       | 0.5527  | 290  | OR2T32P      | 0.5177  |
| 23   | MRGPRX4    | 0.8862  | 90   | OTOP3        | 0.6707  | 157  | KRT14        | 0.6042  | 224  | HOXC4        | 0.5515  | 291  | FCRLB        | 0.5170  |
| 24   | SNORD91A   | 0.8861  | 91   | BMP8B        | 0.6673  | 158  | RASA4        | 0.6040  | 225  | SLC3A1       | 0.5515  | 292  | TMEM183B     | 0.5169  |
| 25   | NOTO       | 0.8811  | 92   | ISL2         | 0.6670  | 159  | GLRA4        | 0.6034  | 226  | MMD2         | 0.5508  | 293  | THY1         | 0.5155  |
| 26   | KRT32      | 0.8781  | 93   | ENTPD2       | 0.6663  | 160  | CHAT         | 0.6033  | 227  | COL28A1      | 0.5498  | 294  | FGF13        | 0.5154  |
| 27   | NCRNA00052 | 0.8666  | 94   | LOC644145    | 0.6660  | 161  | C13orf36     | 0.6030  | 228  | OR2W3        | 0.5496  | 295  | LOC646329    | 0.5141  |
| 28   | OR7E89P    | 0.8631  | 95   | FAM19A3      | 0.6643  | 162  | TTY22        | 0.6019  | 229  | PCSK2        | 0.5490  | 296  | LOC100129726 | 0.5140  |
| 29   | HCRT       | 0.8601  | 96   | OR2T12       | 0.6639  | 163  | POLR3G       | 0.6010  | 230  | MIXL1        | 0.5477  | 297  | SLITRK2      | 0.5140  |
| 30   | MIR3907    | 0.8565  | 97   | FGFBP3       | 0.6628  | 164  | TTC24        | 0.6004  | 231  | CADM3        | 0.5461  | 298  | SHISA3       | 0.5138  |
| 31   | OR2M1P     | 0.8519  | 98   | TUSC5        | 0.6624  | 165  | PRX          | 0.5978  | 232  | BEAN1        | 0.5456  | 299  | TMC3         | 0.5132  |
| 32   | MRGPRX1    | 0.8291  | 99   | CHRNA9       | 0.6583  | 166  | LOC285401    | 0.5971  | 233  | LOC645431    | 0.5454  | 300  | P2RY12       | 0.5124  |
| 33   | MRGPRD     | 0.8071  | 100  | OTOF         | 0.6581  | 167  | PLA2G3       | 0.5957  | 234  | IMPDH1       | 0.5454  | 301  | PRRG3        | 0.5114  |
| 34   | NEFH       | 0.7988  | 101  | ANGPTL7      | 0.6576  | 168  | CCL1         | 0.5939  | 235  | CLDN19       | 0.5443  | 302  | MICALL2      | 0.5112  |
| 35   | MRGPRE     | 0.7926  | 102  | SHOX2        | 0.6566  | 169  | KCND1        | 0.5920  | 236  | LOC200726    | 0.5436  | 303  | COL27A1      | 0.5110  |
| 36   | P2RX3      | 0.7858  | 103  | SLC18A3      | 0.6554  | 170  | COL22A1      | 0.5899  | 237  | FABP7        | 0.5431  | 304  | SLC13A1      | 0.5108  |
| 37   | PSMB11     | 0.7852  | 104  | CALCA        | 0.6553  | 171  | OR2L1P       | 0.5849  | 238  | FAM90A10     | 0.5429  | 305  | CHRN3        | 0.5106  |
| 38   | CST4       | 0.7728  | 105  | PLEKH1D1     | 0.6549  | 172  | RDH12        | 0.5844  | 239  | LOC440300    | 0.5426  | 306  | FKBP1B       | 0.5104  |
| 39   | HOXB8      | 0.7718  | 106  | POU4F1       | 0.6519  | 173  | FMO1         | 0.5841  | 240  | MIA          | 0.5423  | 307  | CCL3L3       | 0.5104  |
| 40   | POU4F3     | 0.7700  | 107  | NPPB         | 0.6511  | 174  | NRG1         | 0.5841  | 241  | PRG1         | 0.5421  | 308  | PCBP3        | 0.5094  |
| 41   | SNAR-B1    | 0.7700  | 108  | IL31RA       | 0.6506  | 175  | OR7E102P     | 0.5840  | 242  | LRRC16B      | 0.5418  | 309  | KCNA6        | 0.5091  |
| 42   | SNAR-B2    | 0.7700  | 109  | DEFB130      | 0.6499  | 176  | LOC647012    | 0.5828  | 243  | TRPV3        | 0.5412  | 310  | GSTT2B       | 0.5084  |
| 43   | FOSB       | 0.7584  | 110  | LOC100133267 | 0.6499  | 177  | AHNAK2       | 0.5827  | 244  | VAMP1        | 0.5405  | 311  | FXYD7        | 0.5083  |
| 44   | LCTL       | 0.7571  | 111  | SCN11A       | 0.6495  | 178  | REEP1        | 0.5815  | 245  | ISL1         | 0.5396  | 312  | C2orf66      | 0.5082  |
| 45   | TMEM132E   | 0.7539  | 112  | GRIK3        | 0.6489  | 179  | STMN2        | 0.5812  | 246  | L1CAM        | 0.5396  | 313  | OR7E59P      | 0.5080  |
| 46   | BHLHA9     | 0.7505  | 113  | FAM70A       | 0.6487  | 180  | LOC100288346 | 0.5809  | 247  | CHRFAM7A     | 0.5392  | 314  | MOS          | 0.5076  |
| 47   | SCGB1C1    | 0.7439  | 114  | AMIGO3       | 0.6471  | 181  | TSPAN11      | 0.5809  | 248  | GPR83        | 0.5390  | 315  | C17orf99     | 0.5076  |
| 48   | NTRK1      | 0.7438  | 115  | LOC574538    | 0.6467  | 182  | CD1E         | 0.5802  | 249  | LOC100129931 | 0.5388  | 316  | PRSS35       | 0.5075  |
| 49   | BARHL1     | 0.7424  | 116  | OR7E130P     | 0.6463  | 183  | PTPN20B      | 0.5801  | 250  | AFAP1L2      | 0.5381  | 317  | AURKB        | 0.5073  |
| 50   | PRDM12     | 0.7422  | 117  | TAC1         | 0.6449  | 184  | HTR3A        | 0.5800  | 251  | PDZD7        | 0.5377  | 318  | LOC100130148 | 0.5067  |
| 51   | FRMPD1     | 0.7377  | 118  | BET3L        | 0.6440  | 185  | NMB          | 0.5794  | 252  | GNG3         | 0.5372  | 319  | LRRTM1       | 0.5066  |
| 52   | OR2T8      | 0.7376  | 119  | SFRP4        | 0.6435  | 186  | PCDH8        | 0.5786  | 253  | GJC3         | 0.5371  | 320  | HOXA6        | 0.5065  |
| 53   | AVIL       | 0.7362  | 120  | NEFM         | 0.6423  | 187  | AQP12B       | 0.5781  | 254  | CRYGD        | 0.5369  | 321  | CYP1A1       | 0.5064  |
| 54   | TRIM67     | 0.7359  | 121  | POU4F2       | 0.6412  | 188  | OR2A13P      | 0.5766  | 255  | SNORD116-20  | 0.5365  | 322  | PTPRN        | 0.5062  |
| 55   | NBPF24     | 0.7344  | 122  | MAST1        | 0.6374  | 189  | HMX1         | 0.5754  | 256  | RAB3D        | 0.5365  | 323  | LOC100130954 | 0.5041  |
| 56   | DRGX       | 0.7271  | 123  | NGFR         | 0.6374  | 190  | BTNL2        | 0.5754  | 257  | CPEB1        | 0.5363  | 324  | C17orf102    | 0.5039  |
| 57   | TMEM179    | 0.7192  | 124  | TUBB3        | 0.6367  | 191  | ADIPOQ       | 0.5754  | 258  | IFITM5       | 0.5358  | 325  | C1orf130     | 0.5035  |
| 58   | GFRA3      | 0.7188  | 125  | KCNH6        | 0.6356  | 192  | TMEM63C      | 0.5747  | 259  | CYP2W1       | 0.5356  | 326  | COL5A3       | 0.5035  |
| 59   | NEFL       | 0.7183  | 126  | VSTM5        | 0.6354  | 193  | PRIMA1       | 0.5718  | 260  | PODNL1       | 0.5344  | 327  | FBXO2        | 0.5034  |
| 60   | OR11H2     | 0.7176  | 127  | MPZ          | 0.6344  | 194  | OR7E163P     | 0.5713  | 261  | KIF3C        | 0.5337  | 328  | OR6B2        | 0.5022  |
| 61   | CER1       | 0.7153  | 128  | OR1H1P       | 0.6329  | 195  | CHRNA7       | 0.5706  | 262  | ADAMTSL1     | 0.5336  | 329  | MATN2        | 0.5021  |
| 62   | MIR570     | 0.7149  | 129  | LOC149134    | 0.6309  | 196  | EXTL1        | 0.5682  | 263  | BCAN         | 0.5335  | 330  | SLC17A6      | 0.5014  |
| 63   | SHH        | 0.7125  | 130  | AQP12A       | 0.6266  | 197  | CLDN22       | 0.5679  | 264  | DPYSL5       | 0.5313  | 331  | CYSLTR2      | 0.5013  |
| 64   | STAC       | 0.7121  | 131  | KCTD8        | 0.6251  | 198  | SCN4B        | 0.5672  | 265  | HKDC1        | 0.5308  | 332  | B4GALNT4     | 0.5008  |
| 65   | MIR770     | 0.7100  | 132  | TMEM233      | 0.6228  | 199  | CYNE6        | 0.5667  | 266  | CLEC2L       | 0.5298  |      |              |         |
| 66   | FLJ46446   | 0.7017  | 133  | LOC284233    | 0.6224  | 200  | SYNGR3       | 0.5663  | 267  | DISP2        | 0.5288  |      |              |         |
| 67   | LOC727677  | 0.6995  | 134  | TMPRSS5      | 0.6212  | 201  | MIR339       | 0.5653  | 268  | DHH          | 0.5286  |      |              |         |

Supplementary Table 2 GPCRs expression profiling in human DRG

| Rank | GPCR           | DRG/All      | Rank | GPCR    | DRG/All | Rank | GPCR        | DRG/All | Rank | GPCR      | DRG/All | Rank | GPCR    | DRG/All |
|------|----------------|--------------|------|---------|---------|------|-------------|---------|------|-----------|---------|------|---------|---------|
| 1    | <b>GPR139</b>  | <b>0.887</b> | 75   | UTS2R   | 0.237   | 149  | BAI2        | 0.132   | 223  | GPRC5B    | 0.065   | 298  | GPR39   | 0.017   |
| 2    | <b>MRGPRX4</b> | <b>0.886</b> | 76   | HTR1B   | 0.235   | 150  | HTR1F       | 0.131   | 224  | GPR125    | 0.062   | 299  | TSHR    | 0.015   |
| 3    | <b>MRGPRX1</b> | <b>0.829</b> | 77   | CXCR3   | 0.235   | 151  | P2RY11      | 0.131   | 225  | ADRA2B    | 0.062   | 300  | HCA3    | 0.014   |
| 4    | <b>MRGPRD</b>  | <b>0.807</b> | 78   | OPRL1   | 0.233   | 152  | ADORA1      | 0.131   | 226  | F2R       | 0.060   | 301  | RXFP1   | 0.012   |
| 5    | <b>MRGPRE</b>  | <b>0.793</b> | 79   | GABBR1  | 0.229   | 153  | GPR45       | 0.129   | 227  | GPR88     | 0.058   | 302  | CHRM5   | 0.011   |
| 6    | <b>PROKR2</b>  | <b>0.608</b> | 80   | PTGER3  | 0.228   | 154  | GPR12       | 0.129   | 228  | GPR84     | 0.054   | 303  | FFAR2   | 0.011   |
| 7    | <b>NPSR1</b>   | <b>0.607</b> | 81   | LPHN3   | 0.222   | 155  | ADRA2C      | 0.128   | 229  | GRM2      | 0.054   | 304  | GPR182  | 0.010   |
| 8    | <b>FZD2</b>    | <b>0.606</b> | 82   | CELSR2  | 0.221   | 156  | LPAR6       | 0.127   | 230  | RHOD      | 0.054   | 305  | CXCR1   | 0.009   |
| 9    | <b>CHRM4</b>   | <b>0.563</b> | 83   | GPR132  | 0.219   | 157  | PTGER1      | 0.126   | 231  | ADCYAP1R1 | 0.053   | 306  | GPR97   | 0.008   |
| 10   | <b>LPAR3</b>   | <b>0.562</b> | 84   | GPR56   | 0.214   | 158  | LPAR2       | 0.125   | 232  | GPR22     | 0.052   | 307  | CXCR2   | 0.007   |
| 11   | <b>GRM4</b>    | <b>0.560</b> | 85   | PTGER2  | 0.214   | 159  | ADRB2       | 0.123   | 233  | GPR135    | 0.052   | 308  | F2RL3   | 0.006   |
| 12   | <b>F2RL2</b>   | <b>0.556</b> | 86   | GPR61   | 0.210   | 160  | HTR4        | 0.123   | 234  | CHRM3     | 0.050   | 309  | NTSR1   | 0.005   |
| 13   | <b>GPR149</b>  | <b>0.555</b> | 87   | GPR64   | 0.209   | 161  | ADORA2B     | 0.122   | 235  | FPR1      | 0.050   | 310  | GRM3    | 0.004   |
| 14   | <b>GPR83</b>   | <b>0.539</b> | 88   | BOKRB2  | 0.209   | 162  | GPR75       | 0.119   | 236  | SSTR3     | 0.050   | 311  | GRM5    | 0.004   |
| 15   | <b>P2RY12</b>  | <b>0.512</b> | 89   | GPR142  | 0.208   | 163  | <b>TGR5</b> | 0.117   | 237  | GPR15     | 0.050   | 312  | S1PR5   | 0.002   |
| 16   | <b>CYSLTR2</b> | <b>0.501</b> | 90   | P2RY1   | 0.207   | 164  | CRCP        | 0.116   | 238  | S1PR4     | 0.049   | 313  | ADRB3   | 0.000   |
| 17   | HTR1D          | 0.489        | 91   | GPR98   | 0.204   | 165  | GPR176      | 0.114   | 239  | LPHN2     | 0.049   | 314  | AGTR2   | 0.000   |
| 18   | GPR114         | 0.487        | 92   | PTGER4  | 0.199   | 166  | NMUR1       | 0.114   | 240  | OXTR      | 0.049   | 315  | AVPR1B  | 0.000   |
| 19   | GPR173         | 0.482        | 93   | GPR152  | 0.196   | 167  | MCHR1       | 0.114   | 241  | FZD9      | 0.048   | 316  | BR3     | 0.000   |
| 20   | CCKAR          | 0.478        | 94   | HCA1R   | 0.194   | 168  | GNRHR       | 0.112   | 242  | GPR52     | 0.047   | 317  | CCR3    | 0.000   |
| 21   | MC5R           | 0.461        | 95   | LTB4R   | 0.192   | 169  | S1PR2       | 0.111   | 243  | GPR55     | 0.047   | 318  | CCR7    | 0.000   |
| 22   | OPRK1          | 0.457        | 96   | LPHN1   | 0.192   | 170  | GPR183      | 0.110   | 244  | GPR113    | 0.047   | 319  | CCR8    | 0.000   |
| 23   | GPR35          | 0.457        | 97   | GPR133  | 0.191   | 171  | HTR6        | 0.110   | 245  | CCRL2     | 0.046   | 320  | CNR2    | 0.000   |
| 24   | FFAR1          | 0.447        | 98   | P2RY6   | 0.188   | 172  | FZD6        | 0.107   | 246  | GPR179    | 0.046   | 321  | DRD3    | 0.000   |
| 25   | CX3CR1         | 0.445        | 99   | GNRHR2  | 0.187   | 173  | ADORA2A     | 0.104   | 247  | ADRA1B    | 0.045   | 322  | FPR2    | 0.000   |
| 26   | FZD8           | 0.441        | 100  | GPR34   | 0.187   | 174  | GPR25       | 0.102   | 248  | CELSR2    | 0.044   | 323  | GALR3   | 0.000   |
| 27   | GPR27          | 0.440        | 101  | GPR126  | 0.185   | 175  | P2RY2       | 0.102   | 249  | APLNR     | 0.044   | 324  | GHRHR   | 0.000   |
| 28   | LGR5           | 0.436        | 102  | RXFP3   | 0.184   | 176  | GPR65       | 0.102   | 250  | GRM6      | 0.043   | 325  | GHSR    | 0.000   |
| 29   | QRFP           | 0.434        | 103  | NPY5R   | 0.184   | 177  | GPRC5C      | 0.101   | 251  | GPR160    | 0.043   | 326  | GPR101  | 0.000   |
| 30   | GPR128         | 0.426        | 104  | HTR5A   | 0.179   | 178  | C5AR1       | 0.098   | 252  | GIPR      | 0.043   | 327  | GPR110  | 0.000   |
| 31   | LHCSR          | 0.425        | 105  | GPR153  | 0.179   | 179  | FZD3        | 0.098   | 253  | GPR116    | 0.043   | 328  | GPR112  | 0.000   |
| 32   | OPRD1          | 0.416        | 106  | CXCR4   | 0.179   | 180  | PTGIR       | 0.097   | 254  | GPR141    | 0.043   | 329  | GPR119  | 0.000   |
| 33   | PTGFR          | 0.405        | 107  | GPR19   | 0.179   | 181  | P2RY8       | 0.096   | 255  | HTR1E     | 0.043   | 330  | GPR144  | 0.000   |
| 34   | MRGPRX3        | 0.379        | 108  | CRHR1   | 0.177   | 182  | GPR174      | 0.095   | 256  | GPR62     | 0.043   | 331  | GPR148  | 0.000   |
| 35   | MAS1L          | 0.378        | 109  | CCR2    | 0.174   | 183  | PTH2R       | 0.094   | 257  | CCR4      | 0.041   | 332  | GPR150  | 0.000   |
| 36   | NPFRR2         | 0.377        | 110  | GPR17   | 0.173   | 184  | GPR3        | 0.093   | 258  | NMUR2     | 0.041   | 333  | GPR151  | 0.000   |
| 37   | GPR37L1        | 0.373        | 111  | GPR50   | 0.173   | 185  | GPR26       | 0.092   | 259  | HTR2A     | 0.040   | 334  | GPR31   | 0.000   |
| 38   | DRD2           | 0.368        | 112  | CASR    | 0.172   | 186  | GRM8        | 0.092   | 260  | GPR123    | 0.039   | 335  | GPR32   | 0.000   |
| 39   | GPR161         | 0.360        | 113  | TBX2R   | 0.170   | 187  | EMR4P       | 0.091   | 261  | CHRM1     | 0.039   | 336  | GPR6    | 0.000   |
| 40   | PTGDR          | 0.350        | 114  | HRH4    | 0.167   | 188  | NMBR        | 0.090   | 262  | GPR4      | 0.038   | 337  | GPR78   | 0.000   |
| 41   | P2RY14         | 0.335        | 115  | CCR6    | 0.167   | 189  | CXCR6       | 0.089   | 263  | GPR21     | 0.037   | 338  | GPR87   | 0.000   |
| 42   | NPFRR1         | 0.329        | 116  | AVPR2   | 0.167   | 190  | TAS1R3      | 0.088   | 264  | PPYR1     | 0.037   | 339  | GPRC5D  | 0.000   |
| 43   | GRM7           | 0.326        | 117  | CYSLTR1 | 0.166   | 191  | CCR5        | 0.088   | 265  | ELTD1     | 0.036   | 340  | GPRC6A  | 0.000   |
| 44   | HRH1           | 0.320        | 118  | GPR115  | 0.165   | 192  | GPR77       | 0.087   | 266  | EMR1      | 0.036   | 341  | HCRTR1  | 0.000   |
| 45   | CRHR2          | 0.317        | 119  | CALCR   | 0.161   | 193  | FZD4        | 0.087   | 267  | FZD5      | 0.033   | 342  | HTR1A   | 0.000   |
| 46   | FZD1           | 0.313        | 120  | GPR68   | 0.159   | 194  | SSBP1       | 0.086   | 268  | LTB4R2    | 0.033   | 343  | KISS1R  | 0.000   |
| 47   | SSTR4          | 0.311        | 121  | TRIM5   | 0.158   | 195  | CCRL1       | 0.085   | 269  | HCA2R     | 0.032   | 344  | LPAR4   | 0.000   |
| 48   | GPR124         | 0.305        | 122  | TACR1   | 0.157   | 196  | DRD1        | 0.085   | 270  | CALCRL    | 0.032   | 345  | MC2R    | 0.000   |
| 49   | BAI1           | 0.304        | 123  | O3FAR1  | 0.157   | 197  | MC4R        | 0.083   | 271  | F2RL1     | 0.032   | 346  | MC3R    | 0.000   |
| 50   | CCR10          | 0.304        | 124  | CCKBR   | 0.156   | 198  | SSTR2       | 0.082   | 272  | AVPR1A    | 0.031   | 347  | MCHR2   | 0.000   |
| 51   | LPAR5          | 0.298        | 125  | HRH3    | 0.156   | 199  | GPR162      | 0.082   | 273  | GPR37     | 0.028   | 348  | MLNR    | 0.000   |
| 52   | LPAR1          | 0.294        | 126  | GLP1R   | 0.156   | 200  | MTNR1A      | 0.081   | 274  | S1PR1     | 0.028   | 349  | MRGPRG  | 0.000   |
| 53   | DRD4           | 0.293        | 127  | GPR82   | 0.155   | 201  | CCBP2       | 0.080   | 275  | TACR2     | 0.028   | 350  | MRGPRX2 | 0.000   |
| 54   | PROKR1         | 0.291        | 128  | GPR20   | 0.155   | 202  | CCR1        | 0.080   | 276  | SUCNR1    | 0.027   | 351  | MTNR1B  | 0.000   |
| 55   | BAI3           | 0.288        | 129  | CMKLR1  | 0.154   | 203  | HRH2        | 0.079   | 277  | GPR1      | 0.026   | 352  | NPBWR1  | 0.000   |
| 56   | ADRA1D         | 0.287        | 130  | CXCR7   | 0.151   | 204  | BDKRB1      | 0.078   | 278  | CHRM2     | 0.025   | 353  | NPBWR2  | 0.000   |
| 57   | GALR1          | 0.285        | 131  | C3AR1   | 0.150   | 205  | DARC        | 0.077   | 279  | GRM1      | 0.025   | 354  | NPY2R   | 0.000   |
| 58   | FZD7           | 0.282        | 132  | S1PR3   | 0.149   | 206  | GPR111      | 0.076   | 280  | HTR2C     | 0.025   | 355  | OPN5    | 0.000   |
| 59   | GPR156         | 0.281        | 133  | GPR85   | 0.147   | 207  | ADORA3      | 0.075   | 281  | LGR6      | 0.024   | 356  | P2RY10  | 0.000   |
| 60   | P2RY13         | 0.274        | 134  | PTAFR   | 0.147   | 208  | OXGR1       | 0.073   | 282  | EMR3      | 0.024   | 357  | PLHR    | 0.000   |
| 61   | CCR9           | 0.273        | 135  | Tpr1    | 0.147   | 209  | GRPR        | 0.072   | 283  | GPR18     | 0.024   | 358  | RXFP2   | 0.000   |
| 62   | SMO            | 0.270        | 136  | NPY1R   | 0.144   | 210  | MRGPRF      | 0.072   | 284  | GLP2R     | 0.024   | 359  | RXFP4   | 0.000   |
| 63   | P2RY4          | 0.266        | 137  | OXER1   | 0.143   | 211  | HCRTR2      | 0.071   | 285  | AGTR1     | 0.024   | 360  | SSTR5   | 0.000   |
| 64   | GABBR2         | 0.262        | 138  | OPN3    | 0.143   | 212  | CNR1        | 0.070   | 286  | FSHR      | 0.023   | 361  | TAAR3   | 0.000   |
| 65   | FZD10          | 0.260        | 139  | Gpr137  | 0.142   | 213  | MAS1        | 0.070   | 287  | Gpr143    | 0.023   | 362  | TAAR5   | 0.000   |
| 66   | EDNRB          | 0.259        | 140  | EDNRA   | 0.140   | 214  | OPRM1       | 0.070   | 288  | ADRB1     | 0.023   | 363  | TAAR6   | 0.000   |
| 67   | MC1R           | 0.258        | 141  | GPR157  | 0.140   | 215  | C17orf103   | 0.070   | 289  | VIPR1     | 0.023   | 364  | TAAR8   | 0.000   |
| 68   | CELSR3         | 0.257        | 142  | GPR146  | 0.139   | 216  | CD97        | 0.070   | 290  | VIPR2     | 0.022   | 365  | TACR3   | 0.000   |
| 69   | ADRA2A         | 0.252        | 143  | GPFR    | 0.137   | 217  | NTSR2       | 0.067   | 291  | HTR2B     | 0.021   | 366  | TAS1R2  | 0.000   |
| 70   | DRD5           | 0.249        | 144  | GPR63   | 0.136   | 218  | FFAR3       | 0.066   | 292  | CXCR5     | 0.020   | 367  | TRHR    | 0.000   |
| 71   | LGR4           | 0.242        | 145  | TAS1R1  | 0.134   | 219  | CTSR        | 0.066   | 293  | ADRA1A    | 0.019   | 368  | XCR1    | 0.000   |
| 72   | HTR7           | 0.241        | 146  | NPY6R   | 0.134   | 220  | SSTR1       | 0.066   | 294  | GPRC5A    | 0.018   |      |         |         |
| 73   | GPR158         | 0.240        | 147  | PTH1R   | 0.134   | 221  | EMR2        | 0.066   | 295  | GALR2     | 0.018   |      |         |         |
| 74   | Gpr107         | 0.240        | 148  | FPR3    | 0.133   | 222  | GCGR        | 0.065   | 296  | GPR171    | 0.017   |      |         |         |